Electronic Supplementary Material (ESI) for Chemical Communications.

Electronic Supporting Information

A mononuclear, terminal titanium(III) imido

Jacob S. Mohar,[a] Anders Reinholdt,[a,b] Taylor M. Keller,[a] Patrick J. Carroll,[a] Joshua Telser,[c,*] and Daniel J. Mindiola[a,*]

[a]Department of Chemistry, University of Pennsylvania, 231 S 34th Street Philadelphia, Pennsylvania, United States
[b]Centre for Analysis and Synthesis, Department of Chemistry, Faculty of Science, Naturvetarvägen 14/Sölvegatan 39 A, 223 62 Lund, Sweden
[c]Department of Biological, Physical and Health Sciences, Roosevelt University, Chicago, Illinois 60605, United States
*Corresponding Authors: mindiola@sas.upenn.edu; jtelser@roosevelt.edu

Table of Contents

1. Methods and Materials S5

1.1 General Considerations S5

1.2 Nuclear Magnetic Resonance Spectroscopy (NMR) S5

1.3 Solution State Magnetic Susceptibility S6

1.4 Infrared Spectroscopy S6

1.5 Ultra-Violet-Visible (UV-Vis) Absorption Spectroscopy S6

1.6 Electrochemical Studies S6

1.7 Single Crystal X-ray Diffraction (XRD) S7

1.8 Statement on Elemental Analysis (EA) S7

2. Synthesis S8

2.1 [($Tp^{tBu,Me}$)Ti{≡NSi(CH_3)$_3$}(THF)], **2** S8

2.2 [($Tp^{tBu,Me}$)Ti{≡NSi(CH_3)$_3$}(Cl)], **1** S7

2.3 [($Tp^{tBu,Me}$)TiCl(OEt_2)][B(C_6F_5)$_4$], **3** S8

2.4 [($Tp^{tBu,Me}$)Ti{≡NSi(CH_3)$_3$}(F)], **4** S9

3. NMR Spectroscopy S10

3.1 NMR Spectroscopy of [($Tp^{tBu,Me}$)Ti{≡NSi(CH_3)$_3$}(THF)], **2** S10

S3.1.1 ^{1}H NMR spectrum and structural assignment of resonances of **2** S10

3.2 NMR Spectroscopy of [($Tp^{tBu,Me}$)Ti{≡NSi(CH_3)$_3$}(Cl)], **1** S11

S3.2.1 ^{1}H NMR spectrum of oxidation of **2** with $ClCPh_3$ reaction mixture S11

3.3 NMR Spectroscopy of [($Tp^{tBu,Me}$)TiCl(OEt_2)][B(C_6F_5)$_4$], **3** S12

S3.3.1 ^{1}H NMR spectrum and structural assignment of resonances of **3** S12

3.4 NMR Spectroscopy of [($Tp^{tBu,Me}$)Ti{≡NSi(CH_3)$_3$}(F)], **4** S13

S3.4.1 ^{1}H NMR spectrum and structural assignment of resonances of **4** S13

S3.4.2 ^{13}C{^{1}H} NMR spectrum and structural assignment of resonances of **4** S14

S3.4.3 ^{1}H ^{1}H-COSY NMR spectrum of **4** S15

S3.4.4 ^{1}H ^{13}C-HSQC NMR spectrum of **4** S16

S3.4.5 ^{1}H ^{13}C-HMBC NMR spectrum of **4** S17

S3.4.6 ^{19}F{^{1}H} NMR spectrum of **4** S18

S3.4.7 ^{29}Si-INEPT NMR spectrum of **4** S19

S3.4.8 ^{11}B{^{1}H} NMR spectrum of **4** S20

S3.4.9 ^{1}H NMR spectrum of **4** over 18 h at 70 °C S21

S3.4.10 ^{19}F{^{1}H} NMR spectrum of **4** over 18 h at 70 °C S22

4. IR Spectroscopy S23

4.1 IR Spectroscopy of [($Tp^{tBu,Me}$)Ti{≡NSi(CH_3)$_3$}(THF)], **2** S23
S4.1.1 IR spectrum of **2** S23
4.2 IR Spectroscopy of [($Tp^{tBu,Me}$)TiCl(Solvent)][B(C_6F_5)$_4$], $\mathbf{3^{Sol}}$ S24
S4.2.1 IR spectrum of $\mathbf{3^{Sol}}$ S24
4.3 IR Spectroscopy of [($Tp^{tBu,Me}$)Ti{≡NSi(CH_3)$_3$}(F)], **4** S25
S4.3.1 IR spectrum of **4** S25
5. UV-Vis Absorbance Spectroscopy S26
5.1 Table of concentrations for Figure 3 in manuscript S26
S5.1.1 Table of concentrations for UV-Vis spectra in Figure 3 in manuscript S26
5.2 UV-Vis Spectroscopy of [($Tp^{tBu,Me}$)Ti{≡NSi(CH_3)$_3$}(THF)], **2** S27
S5.2.1 UV-Vis spectrum of **2** S27
5.3 UV-Vis Spectroscopy of [($Tp^{tBu,Me}$)TiCl(Solvent)][B(C_6F_5)$_4$], $\mathbf{3^{Sol}}$ S28
S5.3.1 UV-Vis spectrum of **3-** d-d transitions (high concentration) S28
S5.3.2 UV-Vis spectrum of **3-** full spectrum (low concentration) S28
S5.3.3 UV-Vis spectrum of **3**- d-d transitions in Et_2O S29
5.4 UV-Vis Spectroscopy of [($Tp^{tBu,Me}$)Ti{≡NSi(CH_3)$_3$}(F)], **4** S230
S5.4.1 UV-Vis spectrum of **4-** d-d transitions S30
6. EPR Spectroscopy S31
6.1 EPR Spectroscopy of [($Tp^{tBu,Me}$)Ti{≡NSi(CH_3)$_3$}(THF)], **2** S31
S6.1.1 X-band EPR spectrum of **2** with ^{47,49}Ti modelling S31
S6.1.2 X-band EPR spectrum of **2** solvent dependence S32
S6.1.3 X-band EPR spectrum of **2** at room temperature S33
6.2 EPR Spectroscopy of [($Tp^{tBu,Me}$)TiCl(Solvent)][B(C_6F_5)$_4$], $\mathbf{3^{Sol}}$ S34
S6.2.1 X-band EPR spectrum of $\mathbf{3^{Sol}}$ at room temperature in toluene S34
S6.2.2 X-band EPR spectrum of $\mathbf{3^{Sol}}$ in toluene/Et_2O (1:1 v/v) S35
S6.2.3 X-band EPR spectrum of $\mathbf{3^{Sol}}$ in toluene/THF (1:1 v/v) S36
7. Electrochemical Studies S37
7.1 Cyclic Voltammetry Studies of [($Tp^{tBu,Me}$)Ti{≡NSi(CH_3)$_3$}(Cl)], **1** S37
S7.1.1 CV of **1** at various scan rates S37
S7.1.2 Randles-Sevcik analysis of **1** based on scan rate dependence S38
S7.1.3 Irreversible reduction feature CV of **1** S38
S7.1.4 Irreversible oxidation feature CV of **1** S39
S7.1.5 CV of **1** at 0.5 V/s over 40 sweeps S39
S7.1.6 Table of addition of chloride ions to **1** S40

S7.1.7-11 Scan rate dependence of chloride ions in CV of **1** S40-S42
S7.1.12-15 Chloride concentration dependence in CV of **1** S43-46
S7.1.16 Proposed electrochemical mechanism S47
7.2 Cyclic Voltammetry Studies of [($Tp^{tBu,Me}$)Ti{≡NSi(CH_3)$_3$}(THF)], **2** S48
S7.2.1 CV of **2** at various scan rates S48
S7.2.2 Randles-Sevcik analysis of **2** based on scan rate dependence S49
S7.2.3 CV of small feature present in CV of **2** S49
S7.2.4 CV of **2** including small reduction feature at various scan rates S50
8. Single Crystal X-ray Diffraction Studies S51
S8.1 Table of crystallographic parameters for selected compounds S51
S8.2 Thermal Ellipsoid plot of **3**-THF S52
9. References S53

1. Materials and Methods

1.1 *General Considerations*

All operations were performed in M. Braun gloves boxes (nitrogen or argon atmosphere) or using standard Schlenk techniques. Pentane (Fisher Scientific), hexanes (Fisher Scientific), toluene (Fisher Scientific), tetrahydrofuran (THF, Fisher Scientific), and diethyl ether (Et_2O, Fisher Scientific) were purchased from commercial vendors, thoroughly bubbled with argon, and made anhydrous by passage through columns of activated alumina in a Grubbs-type solvent system. The anhydrous solvents were stored over sodium metal and 4 Å molecular sieves. Benzene-d_6 (Cambridge Isotope Laboratories) was stored over potassium mirror overnight, sublimed by trap-to-trap transfer *in vacuo*, and degassed by freeze-pump-thaw cycles prior to use. Celite, and 4 Å molecular sieves were activated *in vacuo* overnight at 200 °C.

$[K(Tp^{tBu,Me})]$,[1] $[Tl(Tp^{tBu,Me})]$,[1] $[TiCl_3(THF)_3]$,[2] $[(Tp^{tBu,Me})TiCl_2]$,[3] $[(Tp^{tBu,Me})TiCl]$,[3] [Tl][OTf],[4] and $[KC_8]$[5] were prepared according to reported procedures.

Trimethylsilyl azide (Me_3SiN_3) was purchased from TCI America and degassed by freeze-pump-thaw cycles before use. Trityl chloride ($ClCPh_3$) was purchased from TCI America and was dried *in vacuo* at 80 °C overnight prior to use. Xenon difluoride (XeF_2) was purchased from TCI America and dried *in vacuo* at room temperature for 2 days prior to use.

Thallium tetrakis(pentafluorophenyl)borate, $[Tl][B(C_6F_5)_4]$, was prepared by a modified procedure.[6]

Note: Pörschke prepared $[Tl][B(C_6F_5)_4]$ in 85% yield in a two-step procedure by converting $[Li(Et_2O)_x][B(C_6F_5)_4]$ into $[H(Et_2O)_2][B(C_6F_5)_4]$ and neutralizing with Tl(OEt).[6] *Our procedure directly converts $[Li(Et_2O)_x][B(C_6F_5)_4]$ and Tl(OTf) into $[Tl][B(C_6F_5)_4]$ in near quantitative yield.*

Under nitrogen, to a suspension of Tl(OTf) (498 mg, 1.41 mmol) in 10 ml diethyl ether was added $[Li(Et_2O)_x][B(C_6F_5)_4]$ (1250 mg, x = 3–4, 1.38 mmol, for x = 3), resulting in the dissolution of both reactants. The solution was stirred overnight, while slowly becoming turbid. The suspension was filtered through Celite and concentrated *in vacuo* to leave white solids, $[Tl][B(C_6F_5)_4]$ and [Li][OTf], resulting from metathesis. *[Note: as opposed to $[Li(Et_2O)_x][B(C_6F_5)_4]$, both $[Tl][B(C_6F_5)_4]$ and [Li][OTf] are insoluble in toluene]*. The solids were extracted with dichloromethane (2 × 2 ml), leaving a white insoluble material [Li][OTf], which was removed by filtration through Celite. The filtrate was concentrated *in vacuo*, resulting in an oily residue of $[Tl][B(C_6F_5)_4] \cdot y\ CH_2Cl_2$; the residue crystallizes upon prolonged evacuation, but it can also be crystallized by layering with hexanes followed by storage at –35 °C over 30 minutes. The white microcrystalline solid of $[Tl][B(C_6F_5)_4] \cdot y\ CH_2Cl_2$ was washed with hexanes (3 × 5 ml) and dried *in vacuo*. Yield: 1307 mg. To remove co-crystallized dichloromethane, the white solid was heated to 100 °C in a dynamic vacuum (20 mTorr over 24 h). The resulting loss of mass (CH_2Cl_2) was 138 mg, indicating y = 1.2. Yield of $[Tl][B(C_6F_5)_4]$: 1169 mg, 1.32 mmol, 96.2% (based on $[Li(Et_2O)_x][B(C_6F_5)_4]$, x = 3).

Warning: Tl is highly toxic and it should be handled with extra precaution. All waste containing Tl was handled separately and disposed of properly.

1.2 *Nuclear Magnetic Resonance Spectroscopy (NMR)*

NMR spectroscopic studies were carried out using Bruker 400 MHz or 500 MHz spectrometers equipped with J. Young NMR tubes at room temperature (300 K). ^{1}H and ^{13}C NMR chemical shifts are referenced to the residual solvent signals (C_6D_6: ^{1}H: 7.16 ppm, ^{13}C: 128.06 ppm, THF-d_8: ^{1}H: 1.73 ppm). ^{11}B and ^{19}F chemical shifts are referenced using ^{1}H spectrum as an absolute reference utilizing the IUPAC unified scale which relies on Ξ values expressed as percentages. [7]

1.3 ***Solution State Magnetic Susceptibility***

Magnetic susceptibility was measured by the Evans method[8] in benzene-d_6 or THF-d_8 with the residual protio solvent peak as the internal standard and the deuterated solvent used as the external standard in a capillary. Spin only magnetic values (μ_{eff}) were calculated using the equations shown below. [9] Corrections for diamagnetism were made using tabulated Pascal constants. [10]

$$\frac{3000\Delta f}{4\pi F[M](FW)} = \chi_{measured} \qquad \chi_{mol} = (FW) \times \chi_{measured} \qquad \chi_{P-corr} = \chi_{mol} - \chi_D \qquad \mu_{eff} = 2.84\sqrt{\chi_{P-corr}T}$$

$\Delta f = change\ in\ chemical\ shift\ of\ internal\ and\ external\ standard\ (Hz)$

$F = Instrument\ Frequency\ (Hz)$

$[M] = concentration\ of\ compound\ \left(\frac{mol}{L}\right)$

$FW = molecular\ weight\ of\ compound\ \left(\frac{g}{mol}\right)$

$\chi_D = diamagnetic\ correction\ \left(10^{-6}\frac{emu}{mol}\right)$

$T = Temperature\ (K)$

Calculated Diamagnetic Corrections[10]

Molecular Fragment	$\chi_D\ (10^{-6}\ emu)$
Ti^{III}	-9
$N(Si(CH_3)_3)$	-62.94
$Tp^{tBu,Me}$	-239.07
Cl	-20.1
THF	-41.28
Et_2O	-55.5
BAr_{F20}	-216.76

1.4 ***Infrared Spectroscopy (IR)***

IR spectroscopic studies were carried out using a Jasco FT/IR-4600 spectrometer with samples mounted between KBr windows. The sample chamber was flushed with Ar to prevent decomposition during measurements.

1.5 ***Ultraviolet-Visible Absorption Spectroscopy (UV-Vis)***

UV-Vis spectroscopic studies were carried out using a Cary 5000 Spectrometer equipped with 1 cm quartz cuvettes sealed with J. Young valves.

1.6 ***Electrochemical Studies***

Cyclic voltammetry studies were performed using a CH Instruments 620E Electrochemical Workstation equipped with a three-electrode system: a platinum working electrode, a platinum wire as a counter electrode, and a platinum wire as a reference electrode. Measurements were carried out inside the glovebox. The potentials were referenced to Fc^0/Fc^+ as 0.00 mV. All compounds were recrystallized and dried *in vacuo* twice prior to measurement.

Working and reference electrodes were cleaned and prepared by cycling across the full solvent window 100 times at a scan rate of 0.1 V/s in an electrolyte solution of 0.2 M [^{n}Bu$_4$N][PF$_6$] prior to use. [11]

Tetra-butylammonium hexafluorophosphate [^{n}Bu$_4$N][PF$_6$] was dried *in vacuo* overnight at 100 °C and then brought into the glovebox and recrystallized twice from concentrated THF layered under a small layer of diethyl ether and a large layer of pentane at -35 °C for 12 h. The crystalline material was dried *in vacuo* until it appears as a free-flowing crystalline material prior to use. Tetra-butylammonium chloride [^{n}Bu$_4$N][Cl] was dried *in vacuo* at 65 °C for 72 hours, brought into the glovebox under reduced pressure, recrystallized from concentrated THF at -35 °C overnight two times, and dried *in vacuo* until appearing as a free-flowing crystalline material prior to use.

Ferrocene was sublimed twice at 65 °C overnight prior to use and then stored under an inert atmosphere.

1.7 *Single Crystal X-Ray Diffraction (XRD)*

The single crystal samples were coated with paratone oil, mounted at the end of a MiteGen microloop, and placed under a nitrogen stream at 100K. X-ray intensity data were collected on a Rigaku XtaLAB Synergy-i diffractometer[12] equipped with an HPC area detector (HyPix 3000HE) for **2** and a Rigaku XtaLAB Synergy-S diffractometer[12] equipped with an HPC area detector (Dectris Pilatus3 R 200K) for **4** with both employing confocal multilayer optic-monochromated Mo-Kα radiation. X-ray intensity data were collected on a Bruker APEXII CCD[13] area detector for $\mathbf{3^{Et2O}}$ and $\mathbf{3^{THF}}$ employing graphite-monochromated Mo-Kα radiation. $\mathbf{3^{THF}}$ grew as a non-merohedral twin and CELL_NOW[14] was used to index the diffraction images and determine the twinning mechanism. Rotation frames were integrated using CrysAlisPro[12] for **2** and **4**, and SAINT[15] for $\mathbf{3^{Et2O}}$ and $\mathbf{3^{THF}}$, producing a listing of unaveraged F^2 and $\sigma(F^2)$ values. The intensity data were corrected for Lorentz and polarization effects and for absorption using SCALE3 ABSPACK[16] for **2** and **4**, SADABS[17] for $\mathbf{3^{Et2O}}$ and TWINABS[18] for $\mathbf{3^{THF}}$. The structures were solved by dual space methods – SHELXT. [19] Refinements were by full-matrix least squares based on F^2 using SHELXL.[19] The X-ray data for $\mathbf{3^{THF}}$ were corrected for the presence of disordered solvent using SQUEEZE.[20] All reflections were used during refinement. Non-hydrogen atoms were refined anisotropically and hydrogen atoms were refined using a riding model.

1.8 *Statement on Elemental Analysis (EA)*

EA for **2-4** always resulted in low carbon values despite multiple attempts on crystalline samples. This error could be due to partial degradation of extremely sensitive species during shipment and handling or incomplete combustion during the analysis. We are confident through other methods of characterization including NMR, IR, and scXRD that the samples are adequately pure for reported chemistry.[21]

2. Synthesis

2.1 *Synthesis of [(Tp^{tBu,Me})Ti{≡NSi(CH$_3$)$_3$}(THF)],* ***2***

Under a nitrogen atmosphere, KC_8 (42.0 mg, 0.310 mmol) was added as a solid portion to a stirring THF (7 mL) solution of [Tp^{tBu,Me}Ti{≡NSi(CH$_3$)$_3$}(Cl)] [3] (175.6 mg, 0.296 mmol) chilled to -35 °C. The reaction mixture immediately darkened in color and was allowed to stir for 30 min. Volatiles were removed *in vacuo* and the resulting residue was extracted with hexanes. The suspension was filtered over Celite and the volatiles removed *in vacuo* yielding a dark orange powder which can be used without further purification. X-ray quality crystals were grown from the vapor diffusion of a concentrated Et_2O solution and toluene. Yield: 91.0%, 169.6 mg, 0.270 mmol. **^{1}H NMR** (400 MHz, C_6D_6) δ 10.17 (s, 1H, B-H, $\Delta\nu_{1/2}$ = 100.10 Hz), 4.92 (bs, 3H, pyz C-*H*, $\Delta\nu_{1/2}$ = 39.44 Hz), 1.32 (bs, 9H, Me-Pyz, $\Delta\nu_{1/2}$ = 56.78 Hz), 0.17 (bs, 9H, Si*Me$_3$*, $\Delta\nu_{1/2}$ = 100.10 Hz), -2.09 (bs, 27H, ^{t}Bu-Pyz, $\Delta\nu_{1/2}$ = 100.10 Hz). **Magnetic Moment** (Evan's Method, C_6D_6, 300 K): μ_{eff} = 1.85 μ_B. **IR** solid υ (cm^{-1}) 2543 (B-H). **UV-Vis** toluene, λ [nm, ε ($M^{-1}cm^{-1}$)]: 340.5 (1188.9), 450.0 (1555.4), 616.0 (178.8). **τ_5 value:** 0.29. **EA** calculated for $C_{31}H_{57}BN_7OSiTi$: 59.04% C, 9.11% H, 15.55% N; found: multiple attempts did not result in satisfactory results.[21]

2.2 *Synthesis of [(Tp^{tBu,Me})Ti{≡NSi(CH$_3$)$_3$}(Cl)],* ***1***

Method A: Previously reported[1] and utilized for the synthesis of **2**

Method B: Under a nitrogen atmosphere, [Tp^{tBu,Me}Ti{≡NSi(CH$_3$)$_3$}(THF)] (16.0 mg, 0.0254 mmol) was dissolved in C_6D_6 (*ca.* 450 μL) in an NMR tube and $ClCPh_3$ (7.1 mg, 0.0255 mmol) was added as a solid portion. Reaction was allowed to sit at room temperature for 1 h. ^{1}H NMR collected after 1 h showed the presence of Gomberg's dimer, free THF, and [Tp^{tBu,Me}Ti{≡NSi(CH$_3$)$_3$}(Cl)] (*cf.* Figure S3.2.1). Reaction was allowed to sit overnight and then the volatiles were removed *in vacuo*. The resulting residue was extracted with Et_2O and concentrated. Crystalline material grew from Et_2O matched previously reported ^{1}H NMR chemical shifts for [Tp^{tBu,Me}Ti{≡NSi(CH$_3$)$_3$}(Cl)].[3] Yield: 96.7% (isolated), 14.6 mg, 0.0246 mmol.

2.3 *Synthesis of [(Tp^{tBu,Me})TiCl(OEt$_2$)][BAr$_{F20}$],* ***3***

Under an argon atmosphere, thallium tetrakis(pentafluorophenyl)borate ([Tl][BAr$_{F20}$], 100.4 mg, 0.114 mmol) was dissolved in *ca.* 3 mL of Et_2O and added dropwise to a stirring ethereal solution of (Tp^{tBu,Me})TiCl (57.6 mg, 0.114 mmol). The reaction mixture immediately became turbid and the resulting suspension was allowed to stir for 1 h. Upon filtration through Celite, the resulting light blue ethereal solution was concentrated. X-ray quality crystals were grown from vapor diffusion of the diethyl ether solution into toluene at -35 C overnight. Yield: 65.7%, 94.1 mg, 0.0747 mmol. **^{1}H NMR** (400 MHz, THF-*d$_8$*) δ(ppm): 10.93 (bs, 3H, pyz-C*H*, $\Delta\nu_{1/2}$ = 20.68 Hz), 8.40 (bs, 9H, Me-Pyz, $\Delta\nu_{1/2}$ = 161.43 Hz), 5.87 (bs, 1H, B-*H*, $\Delta\nu_{1/2}$ = 44.66 Hz), 1.30 (bs, 27H, ^{t}Bu-Pyz, $\Delta\nu_{1/2}$ = 100.14 Hz). **Magnetic Moment** (Evan's Method, 300 K): μ_{eff} = 1.86 μ_B. **UV-Vis** THF, λ [nm, ε ($M^{-1}cm^{-1}$)]: 261 (10056.75), 585 (16.82). **IR** solid υ (cm^{-1}) 2572 (B-H). **τ_5 value:** 0.45. **EA** calculated for $C_{52}H_{50}B_2ClF_{20}N_6OTi$: 49.57% C, 4.00% H, 6.67% N; found: multiple attempts did not result in satisfactory results.[21]

2.4 *Synthesis of [(Tp^{tBu,Me})Ti{≡NSi(CH$_3$)$_3$}(F)],* ***4***

Under a nitrogen atmosphere, xenon difluoride (8.5 mg, 0.0502 mmol, 0.5 eq) was dissolved in toluene (*ca.* 1 mL) and added dropwise over one minute to stirring [Tp^{tBu,Me}Ti{≡NSi(CH$_3$)$_3$}(THF)] (63.4 mg, 0.101 mmol, 1 eq) in toluene. The reaction mixture turned light green and was allowed to stir for 3 h. The volatiles were then removed *in vacuo* and the resulting residue extracted into pentane. The pentane solution was then filtered over Celite and the volatiles removed *in vacuo* resulting in a yellow-green powder. X-ray quality crystals were grown from the vapor diffusion of diethyl ether into toluene at -35 °C overnight. Yield: 85.6%, 49.7 mg, 0.0861 mmol. **^{1}H NMR** (400 MHz, C_6D_6) δ 5.69 (s, 3H, Pyz-*H*), 4.26 (s, 1H, B-*H*), 1.85 (s, 9H, Pyz-*Me*), 1.76 (s, 27H, Pyz-^{t}*Bu*), 0.43 (s, 9H, Si-*Me$_3$*). **^{13}C{^{1}H} NMR** (101 MHz, C_6D_6) δ 163.99 (^{t}Bu-*Pyz*), 144.97 (Me-*Pyz*), 103.91 (H-*Pyz*), 32.70 (*C*-Me$_3$), 31.30 (^{t}*Bu*), 12.65 (*Me*), 1.82 (Si-*Me$_3$*). **^{19}F{^{1}H} NMR** (376 MHz, C_6D_6) δ 131.34. **^{11}B{^{1}H} NMR** (128 MHz, C_6D_6) δ -9.81. **^{29}Si NMR** (79 MHz, C_6D_6) δ -16.76. **IR** solid υ (cm^{-1}) 2545 (B-H). **τ_5 value:** 0.51. **EA** calculated for $C_{27}H_{49}BFN_7OSiTi$: 56.15% C, 8.56% H, 16.98% N; found: multiple attempts did not result in satisfactory results.[21]

3. NMR Spectroscopy

3.1 *NMR Spectroscopy of [(Tp^{tBu,Me})Ti{≡NSi(CH$_3$)$_3$}(THF)]*

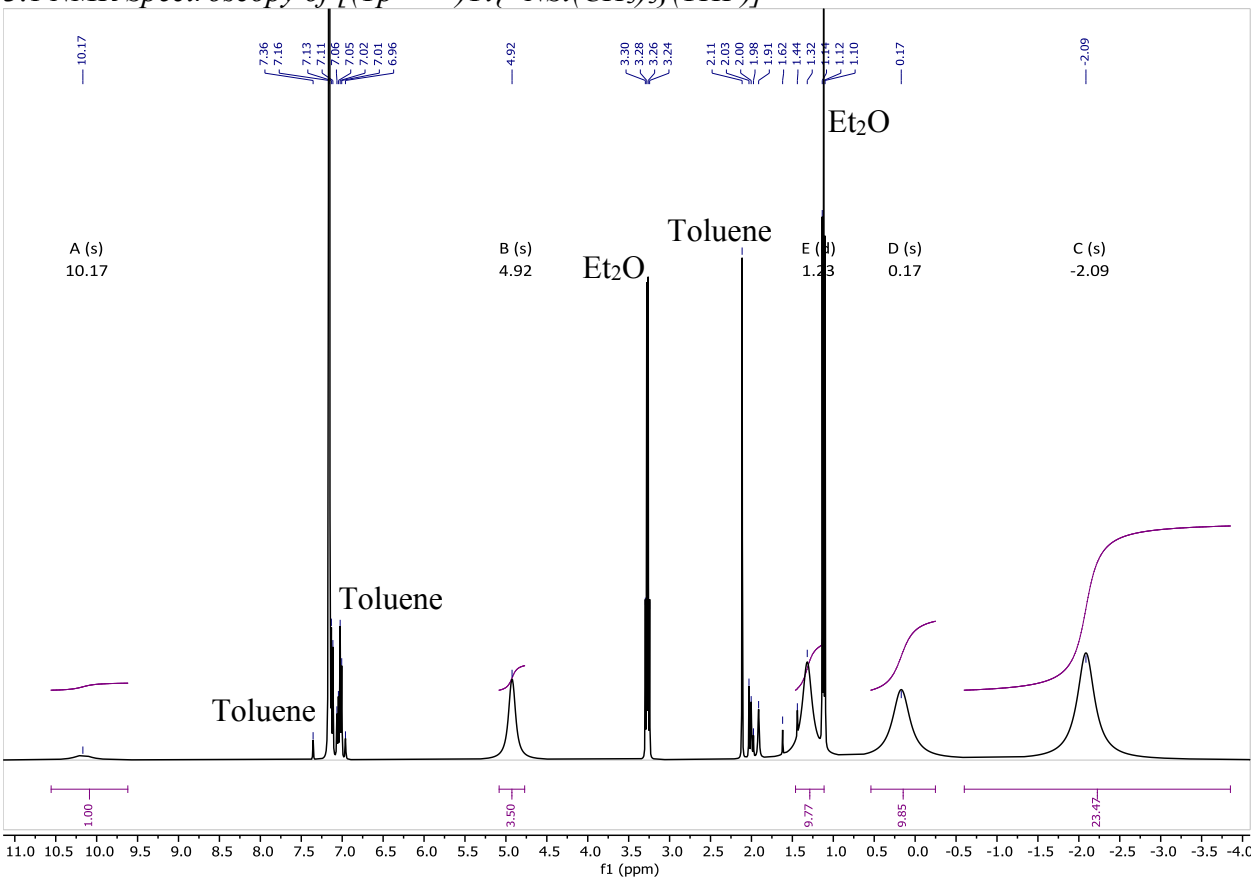

Figure S3.1.1: ^{1}H NMR spectrum of [(Tp^{tBu,Me})Ti{≡NSi(CH$_3$)$_3$}(THF)], **2**, in C_6D_6 and structural assignment of observed resonances. Coordinated THF is found in X-ray structure but not identified in NMR. Stoichiometric THF loss is, however, observed upon oxidation (Figure S3.2.1). Residual solvents shown on spectrum were assigned as previously reported.[22]

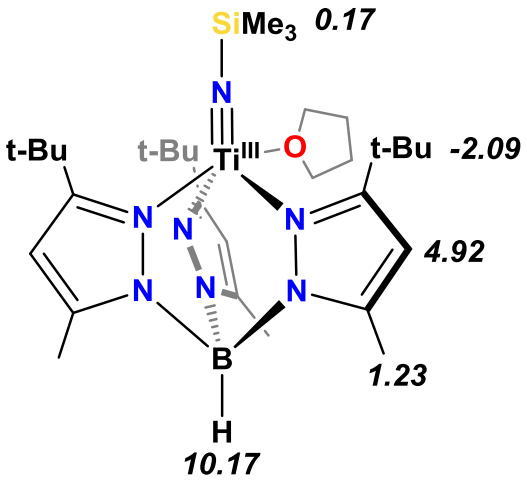

3.2 *NMR Spectroscopy of [(Tp^{tBu,Me})Ti{≡NSi(CH$_3$)$_3$}(Cl)]*

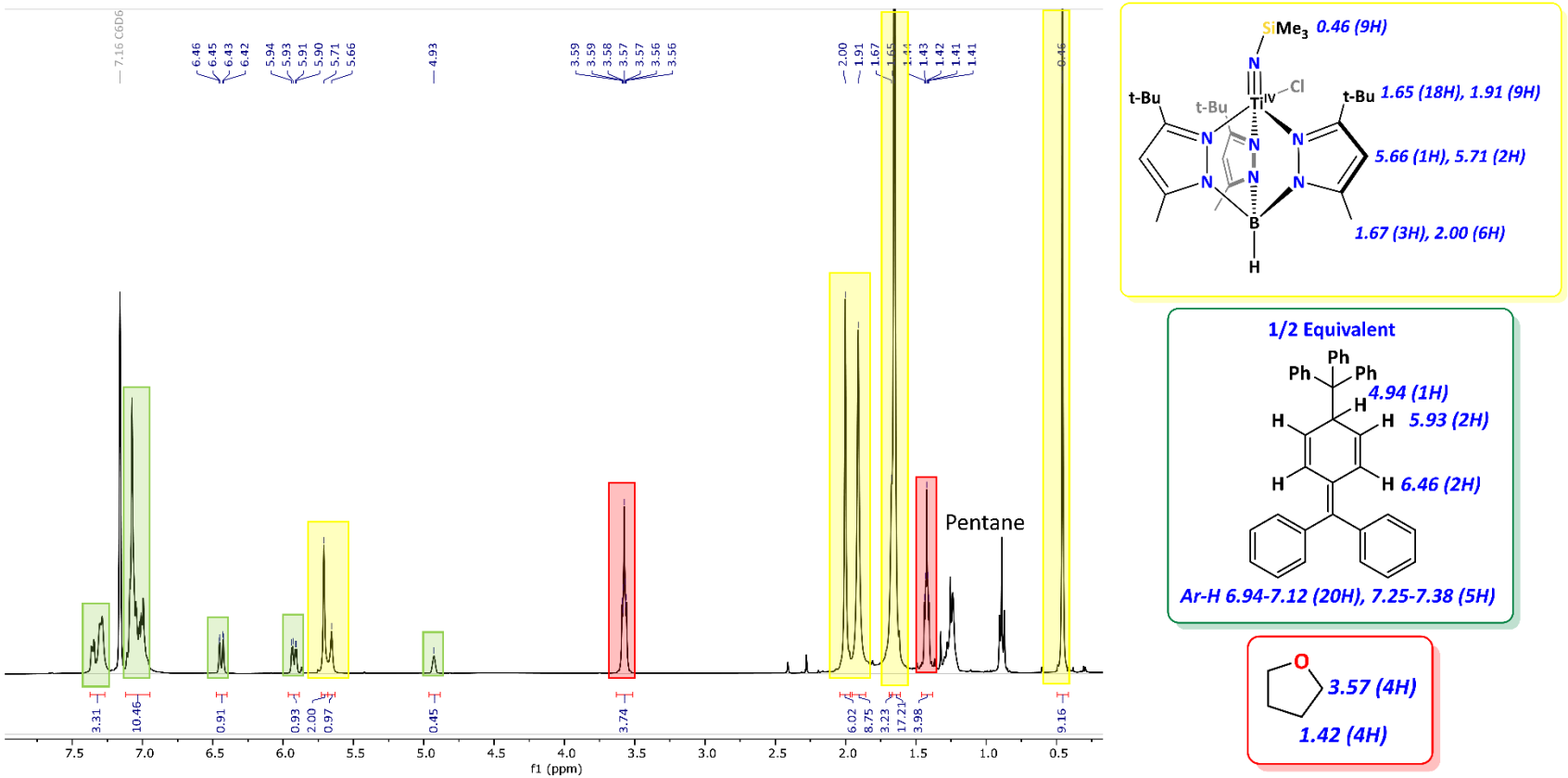

Figure S3.2.1: Monitoring oxidation of **2** *via* ^{1}H NMR spectroscopy. 0.5 equivalent of Gomberg's dimer observed upon oxidation of [(Tp^{tBu,Me})Ti{≡NSi(CH$_3$)$_3$}(THF)], **2**, to [(Tp^{tBu,Me})Ti{≡NSi(CH$_3$)$_3$}(Cl)], **1**, via the addition of ClCPh$_3$.[23] THF comes from the THF-bound to **2**. Integrations standardized to the formation of 1.0 eq. of **1**.[3] Residual THF and pentane resonances have been previously reported.[22]

3.3 *NMR Spectroscopy of [(Tp^{tBu,Me})TiCl(OEt$_2$)][B(C$_6$F$_5$)$_4$]*

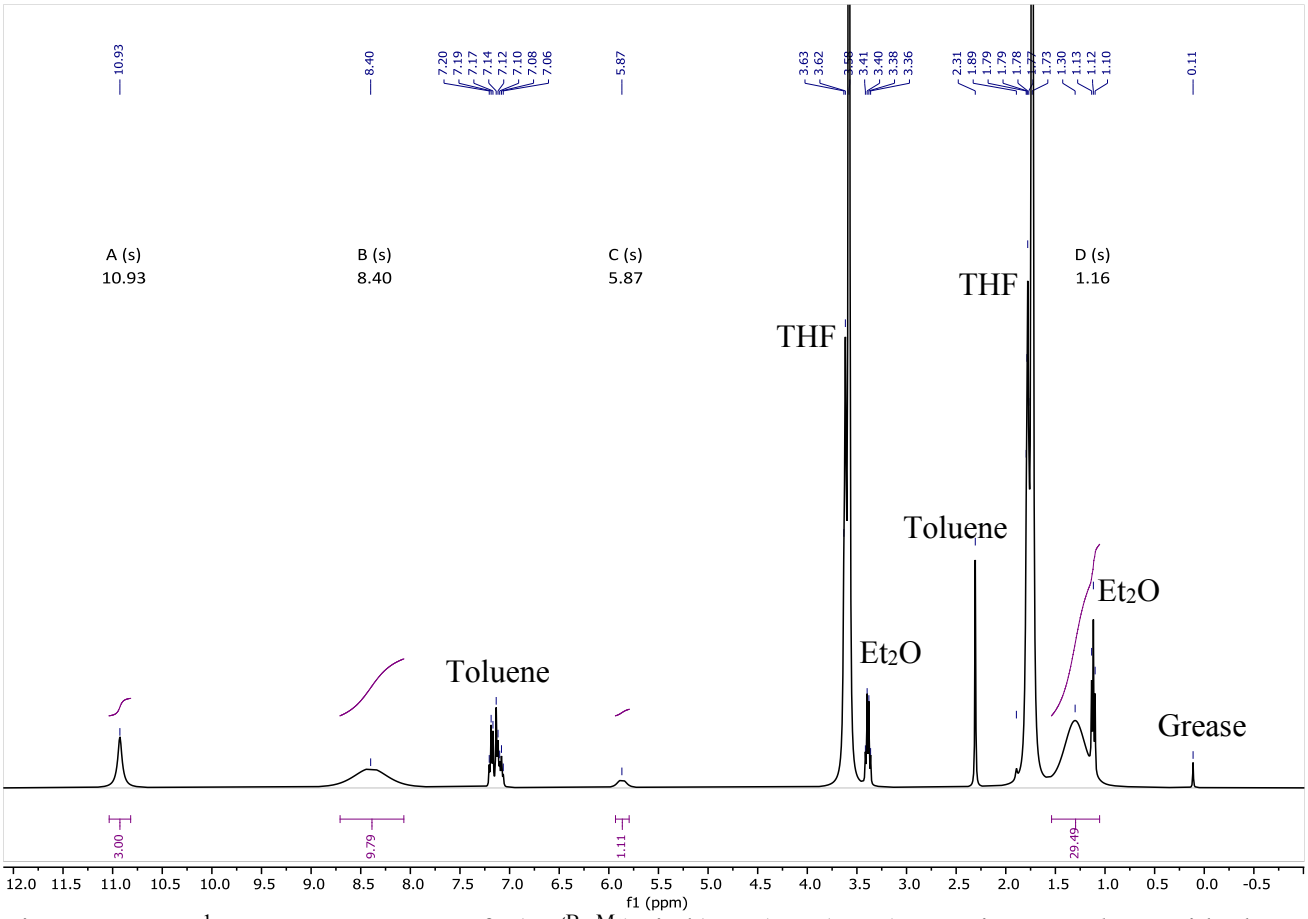

Figure S3.3.1: ^{1}H NMR spectrum of [(Tp^{tBu,Me})TiCl(OEt$_2$)][B(C$_6$F$_5$)$_4$], **3**, in THF-d_8. Residual solvent peaks are labeled in spectrum and were assigned as previously reported.[22] Diethyl ether found as diamagnetic impurity in THF-d_8 but not identified as coordinated to the titanium center by ^{1}H NMR spectroscopy. Structural assignments are made below.

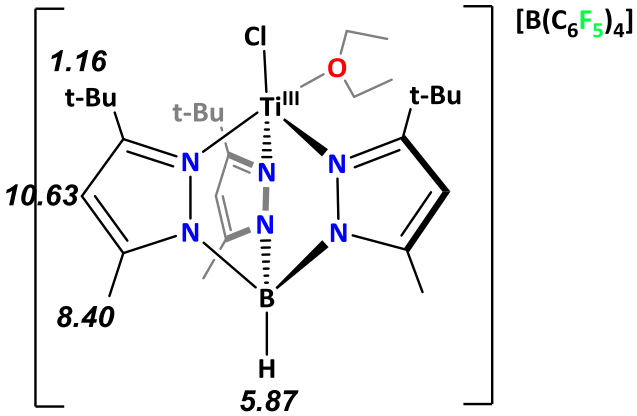

3.4 *NMR Spectroscopy of [(Tp^{tBu,Me})Ti{≡NSi(CH$_3$)$_3$}(F)],* **4**

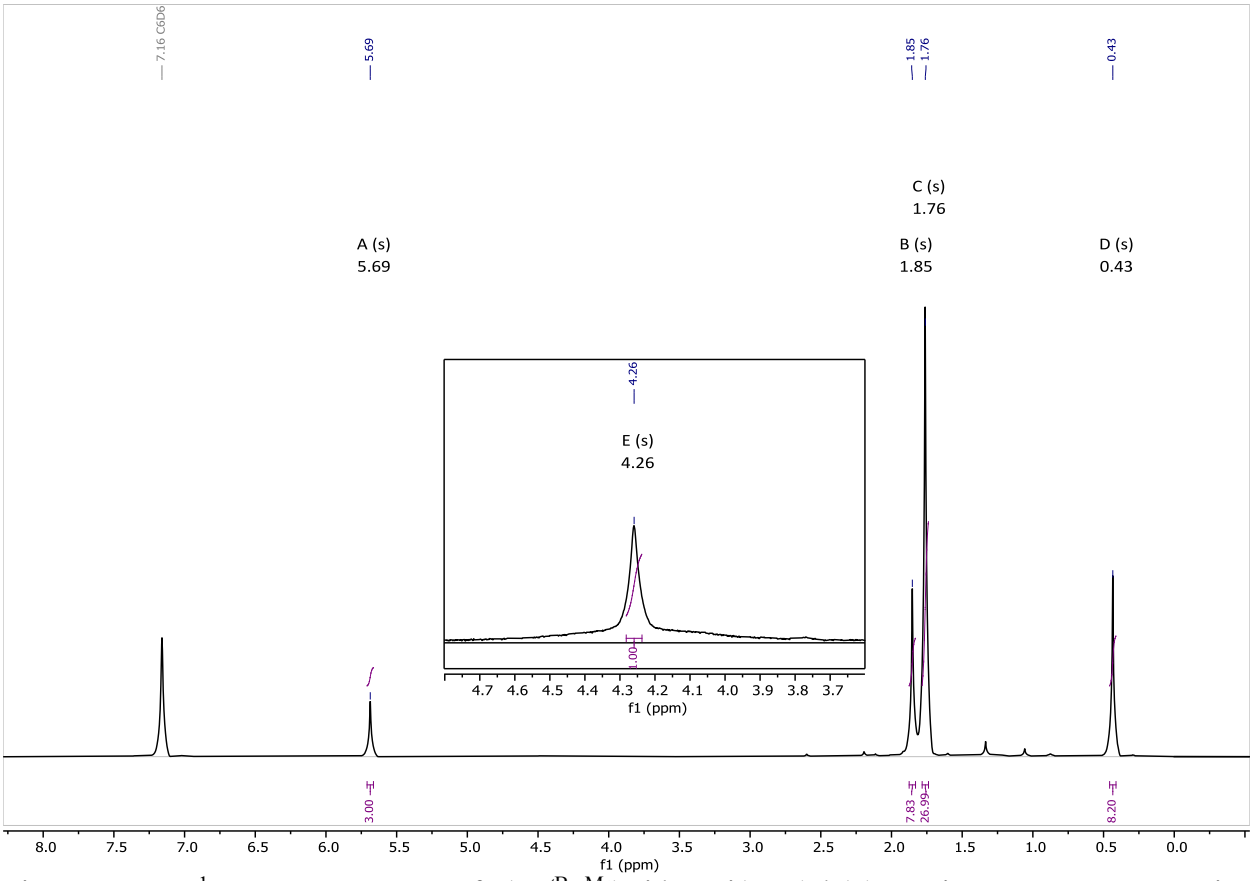

Figure S3.4.1: ^{1}H NMR spectrum of [(Tp^{tBu,Me})Ti{≡NSi(CH$_3$)$_3$}(F)], **4**, in C_6D_6. Insert contains ^{1}H{^{11}B} NMR spectrum. Structural assignments made below.

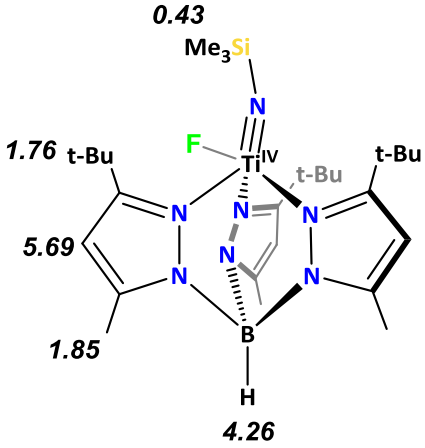

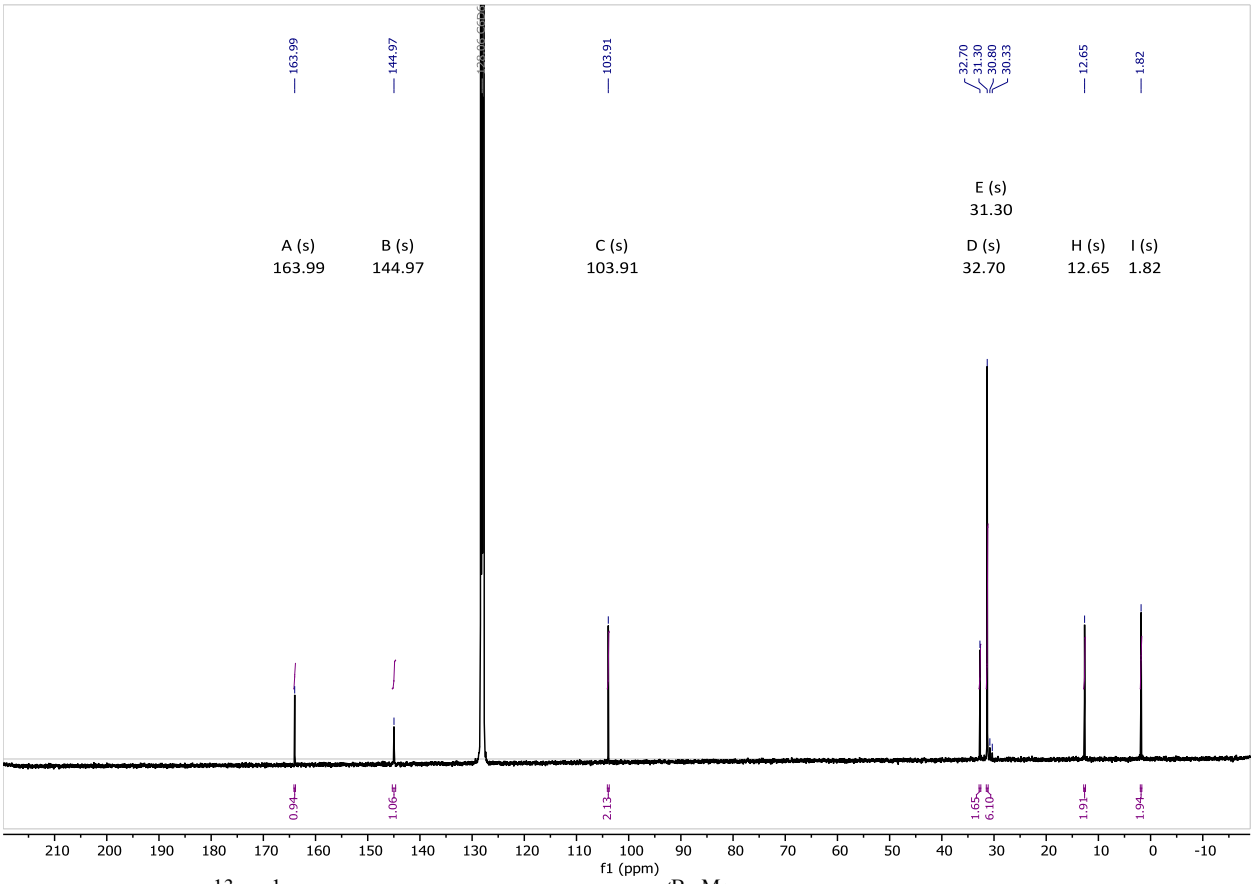

Figure S3.4.2: $^{13}C\{^{1}H\}$ NMR spectrum of [(Tp^{tBu,Me})Ti{≡NSi(CH$_3$)$_3$}(F)], **4**, in C_6D_6 with structural assignments shown below.

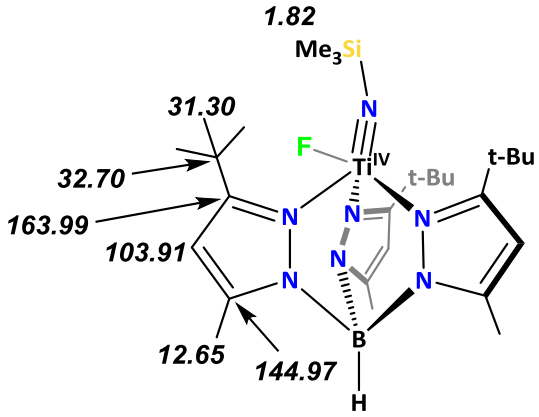

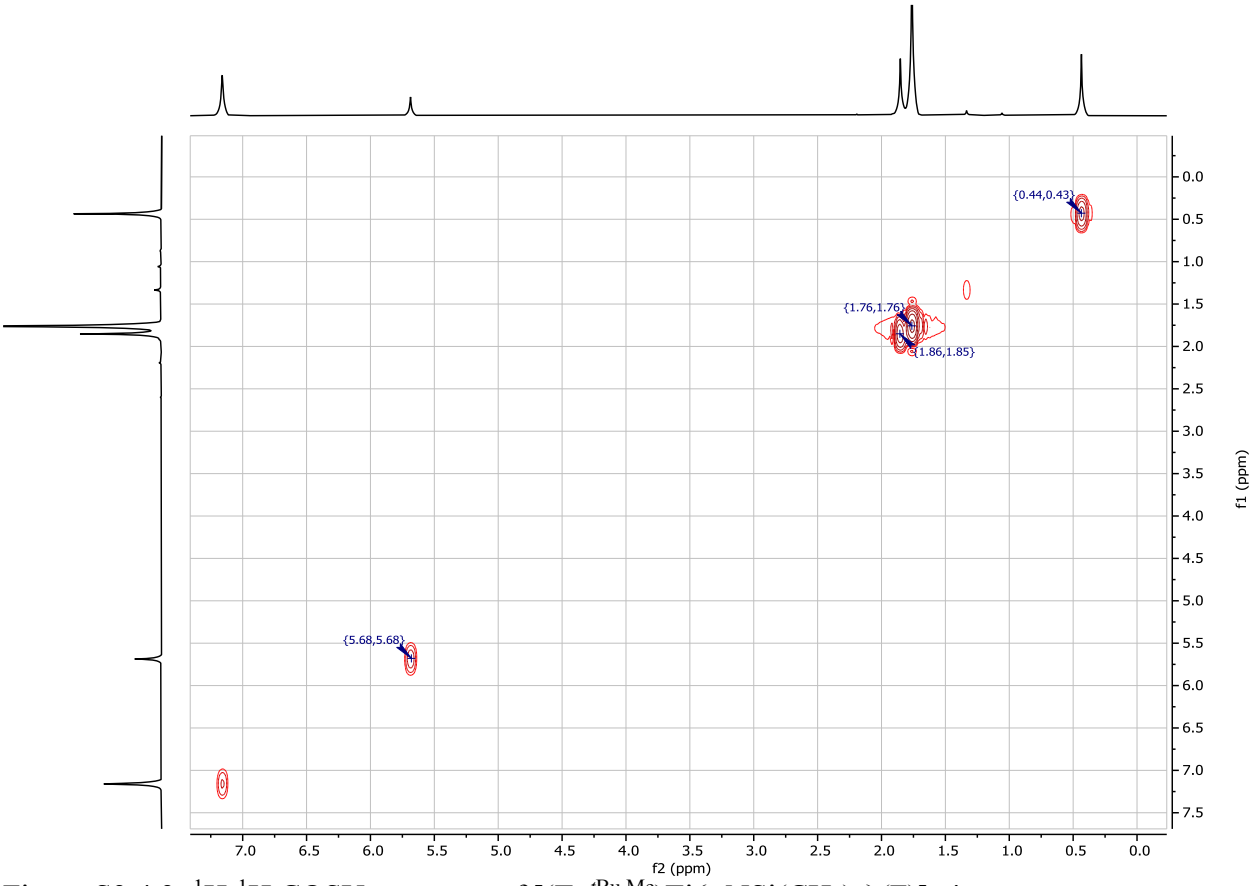

Figure S3.4.3: ^{1}H-^{1}H COSY spectrum of [(Tp$^{t\mathrm{Bu,Me}}$)Ti{≡NSi(CH$_3$)$_3$}(F)], **4**

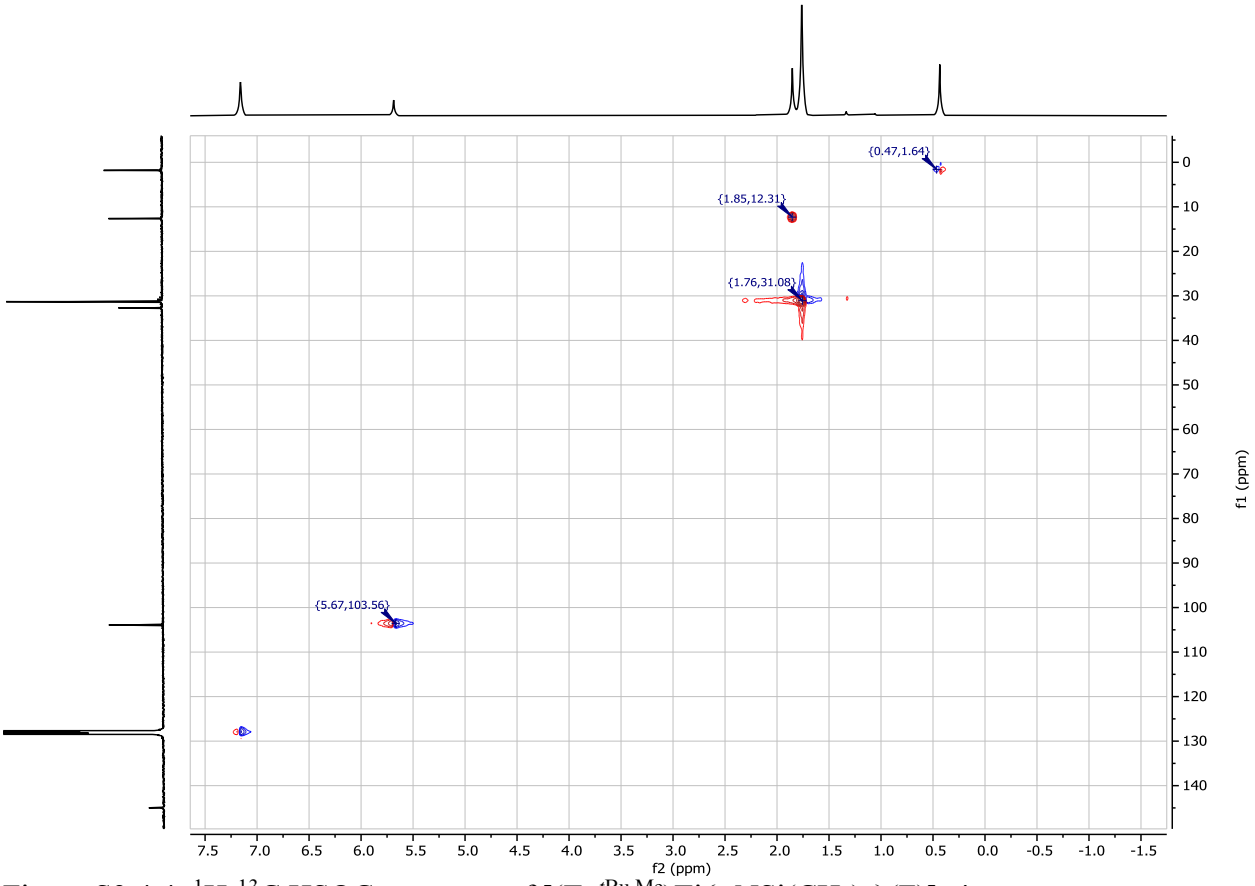

Figure S3.4.4: ^{1}H-^{13}C HSQC spectrum of [(Tp^{tBu,Me})Ti{≡NSi(CH$_3$)$_3$}(F)], **4**

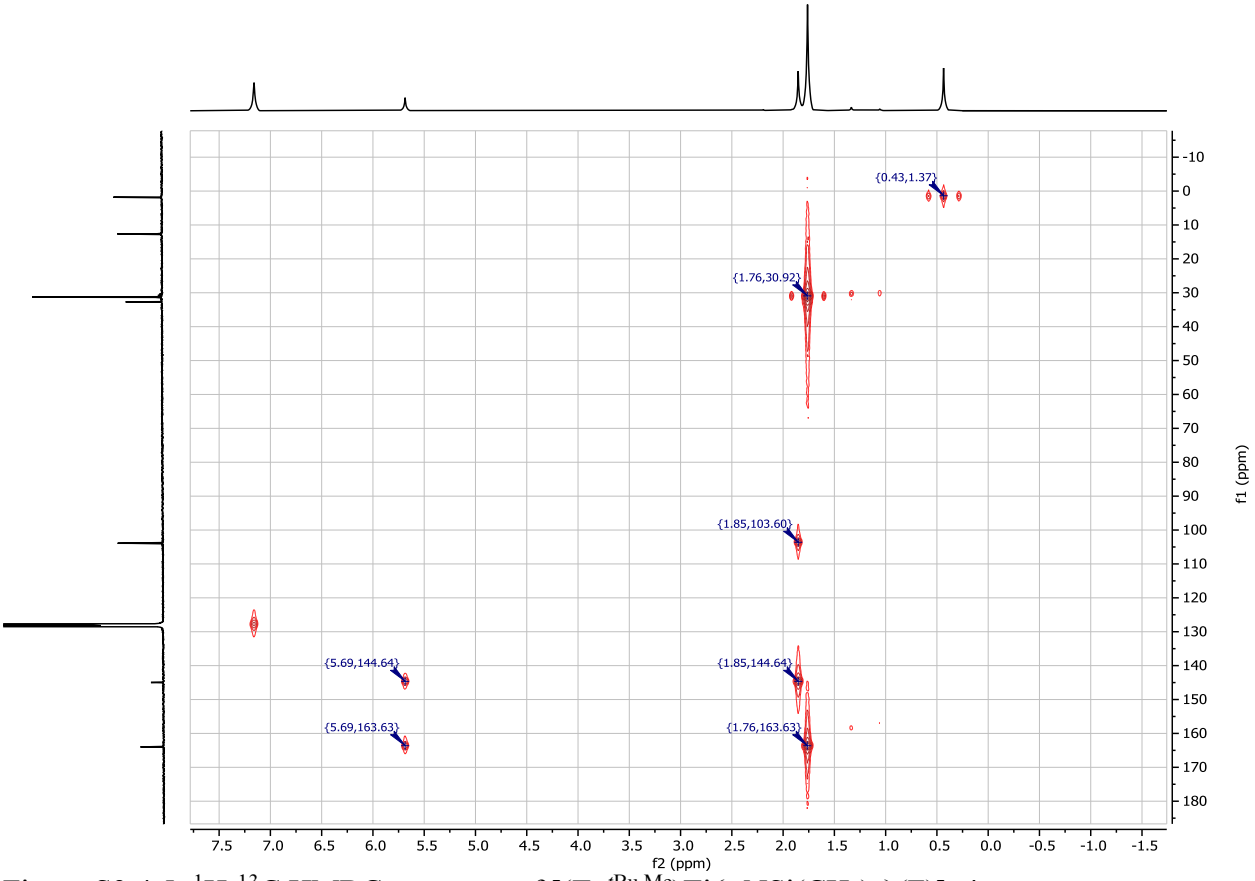

Figure S3.4.5: ^{1}H-^{13}C HMBC spectrum of [(Tp^{tBu,Me})Ti{≡NSi(CH$_3$)$_3$}(F)], **4**

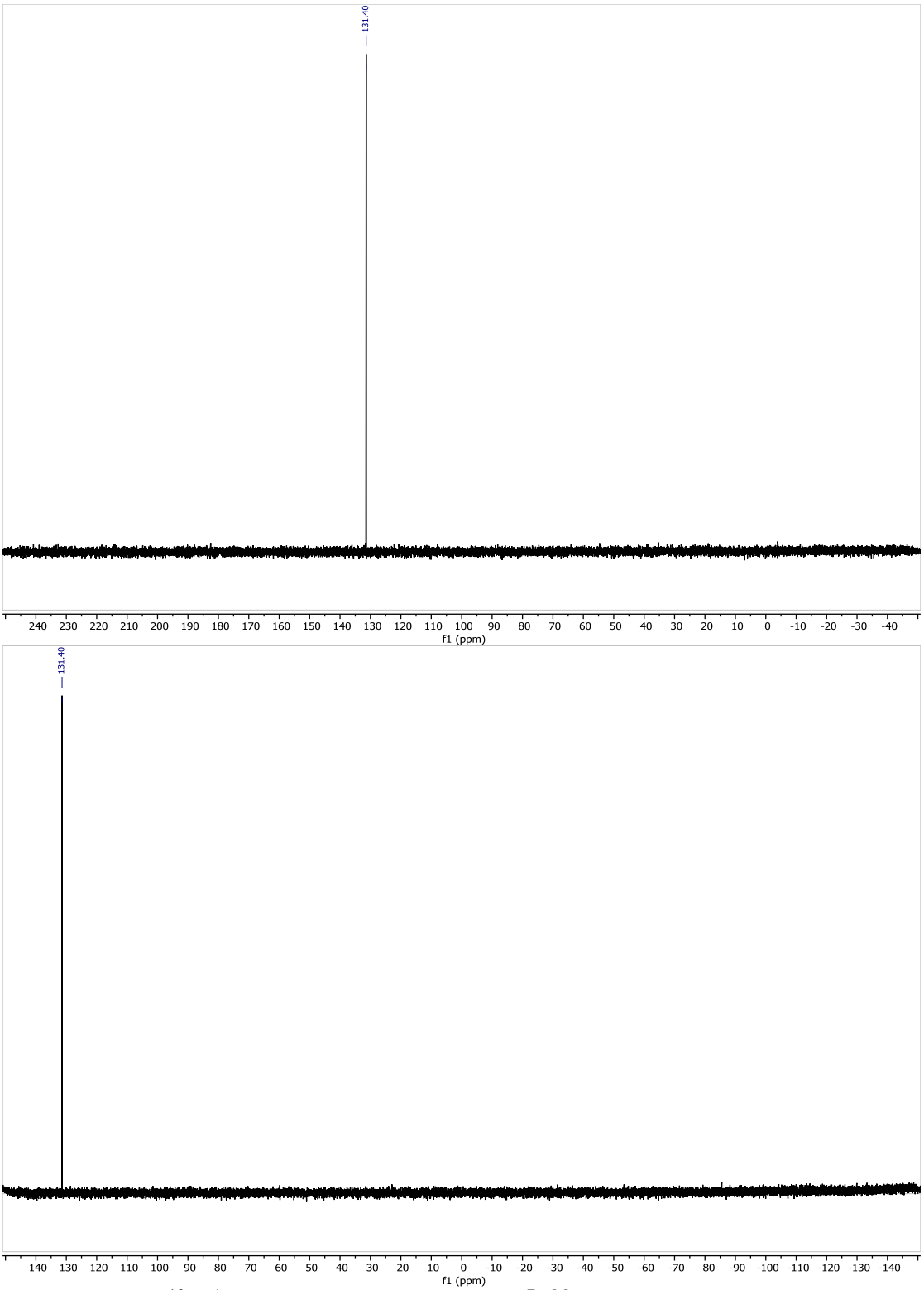

Figure S3.4.6: $^{19}F\{^{1}H\}$ NMR spectrum of [(Tp^{tBu,Me})Ti{≡NSi(CH$_3$)$_3$}(F)], **4**, in C_6D_6 absolute reference[6] to ^{1}H NMR spectrum with two different scan windows.

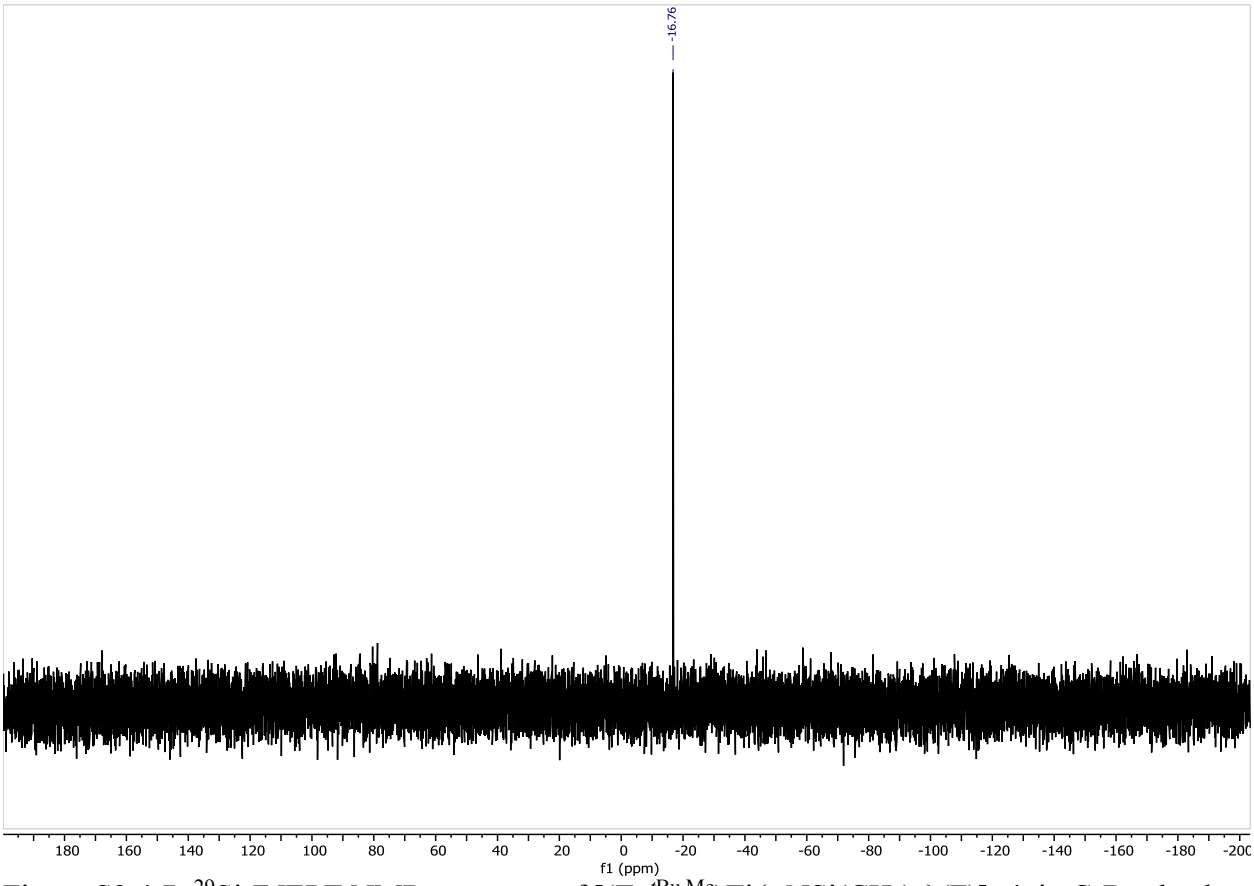

Figure S3.4.7: ^{29}Si-INEPT NMR spectrum of [(Tp^{tBu,Me})Ti{≡NSi(CH$_3$)$_3$}(F)], **4**, in C_6D_6 absolute referenced to ^{1}H spectrum. [6]

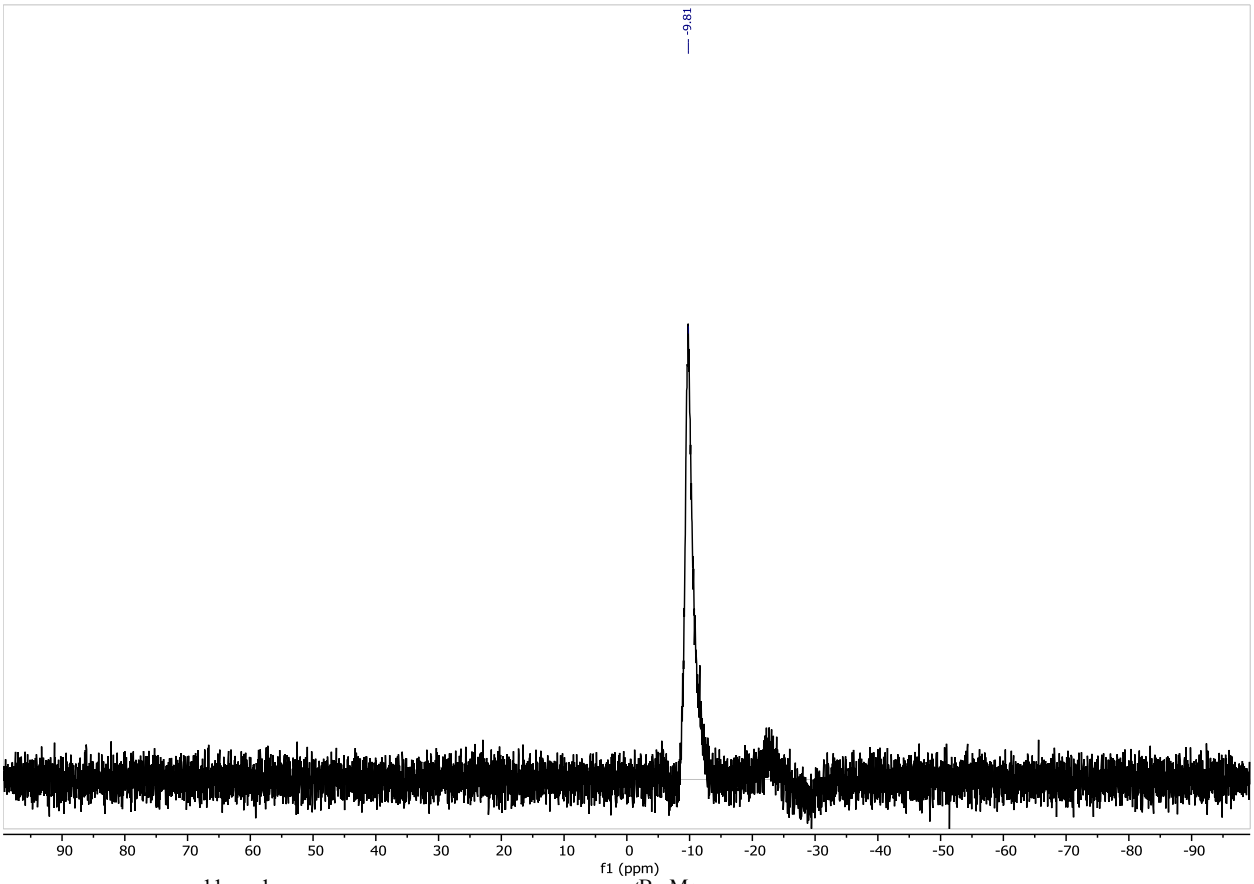

Figure S3.4.8: $^{11}B\{^{1}H\}$ NMR spectrum of [(Tp^{tBu,Me})Ti{≡NSi(CH$_3$)$_3$}(F)], **4**, in C_6D_6 absolute referenced to ^{1}H spectrum. [6]

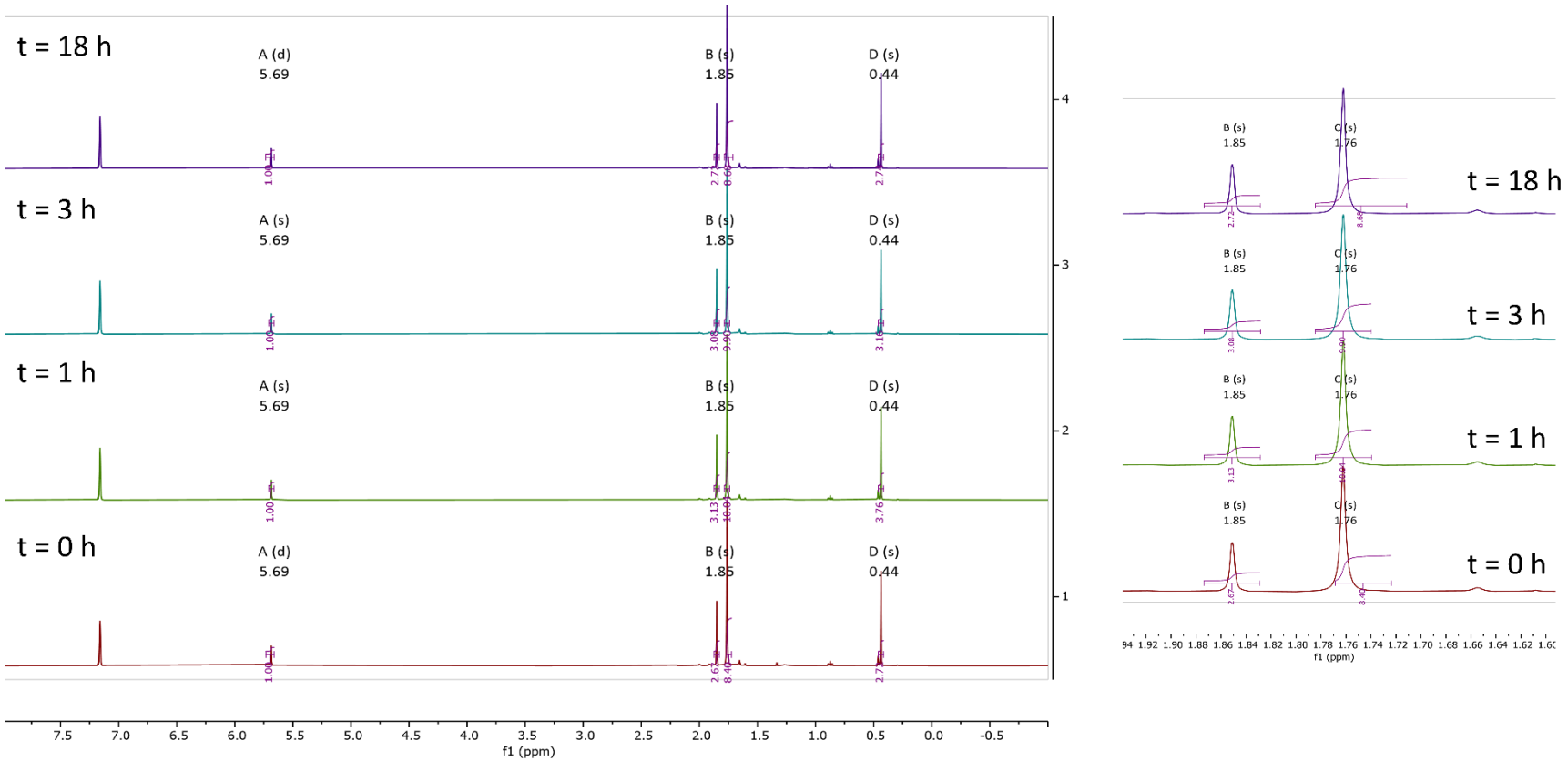

Figure S3.4.9: ^{1}H NMR spectrum of [(Tp$^{t\text{Bu,Me}}$)Ti{≡NSi(CH$_3$)$_3$}(F)], **4**, in C_6D_6 at 70 °C over 18 h to show thermal stability of **4** over time. Insert shows a zoomed in plot of the ^{t}Bu and Me proton resonances to show Berry pseduorotation occurs at high temperature in addition to room temperature.

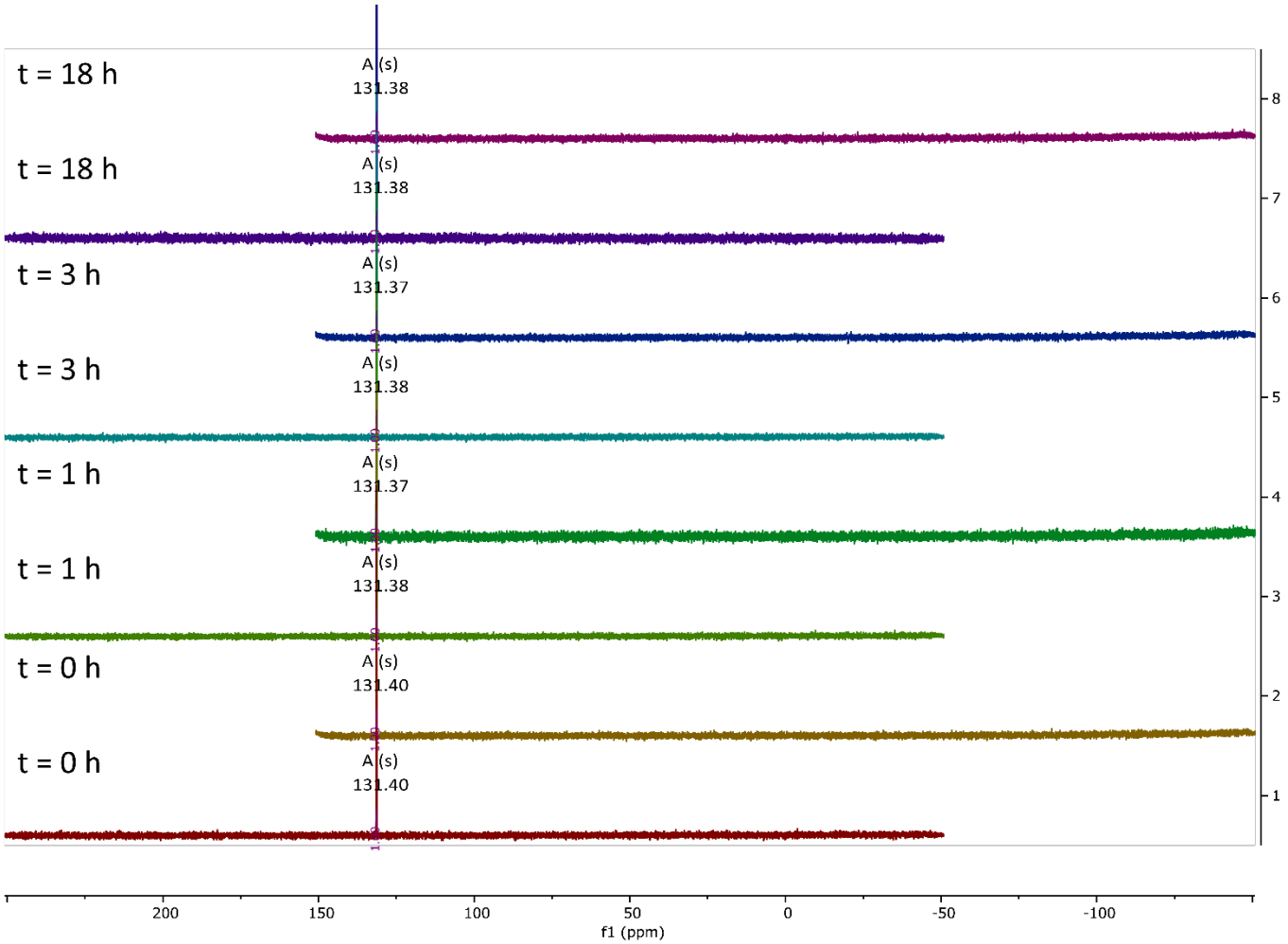

Figure S3.4.10: $^{19}F\{^{1}H\}$ NMR spectrum of [(Tp^{tBu,Me})Ti{≡NSi(CH$_3$)$_3$}(F)], **4**, in C_6D_6 at 70 °C over 18 h to show thermal stability of **4** over time. Spectra absolute referenced to ^{1}H NMR spectrum taken at same time at two different scan windows.[6]

4. IR Spectroscopy

4.1 *IR Spectroscopy of [(Tp^{tBu,Me})Ti{≡NSi(CH$_3$)$_3$}(THF)],* **2**

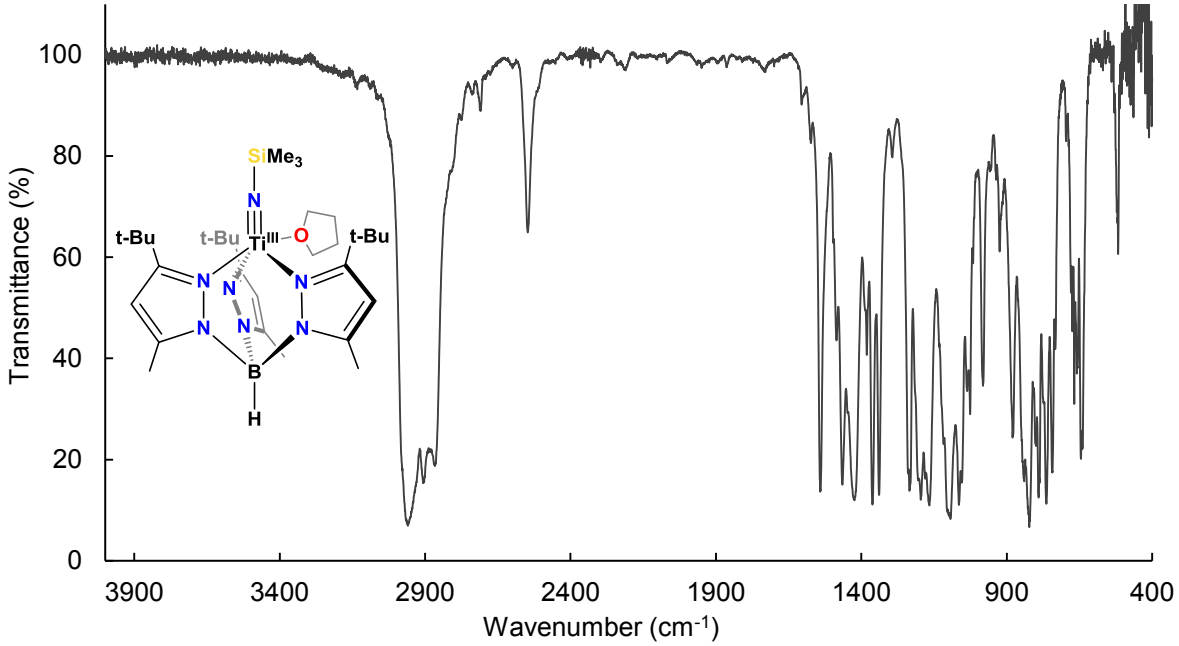

Figure S4.1.1: IR spectrum of solid [(Tp^{tBu,Me})Ti{≡NSi(CH$_3$)$_3$}(THF)], **2**, KBr pellet, cm^{-1}: υ = 2543 (B-H)

4.2 *IR Spectroscopy of* $[(Tp^{tBu,Me})TiCl(OEt_2)][B(C_6F_5)_4]$, $\mathbf{3}^{Et2O}$

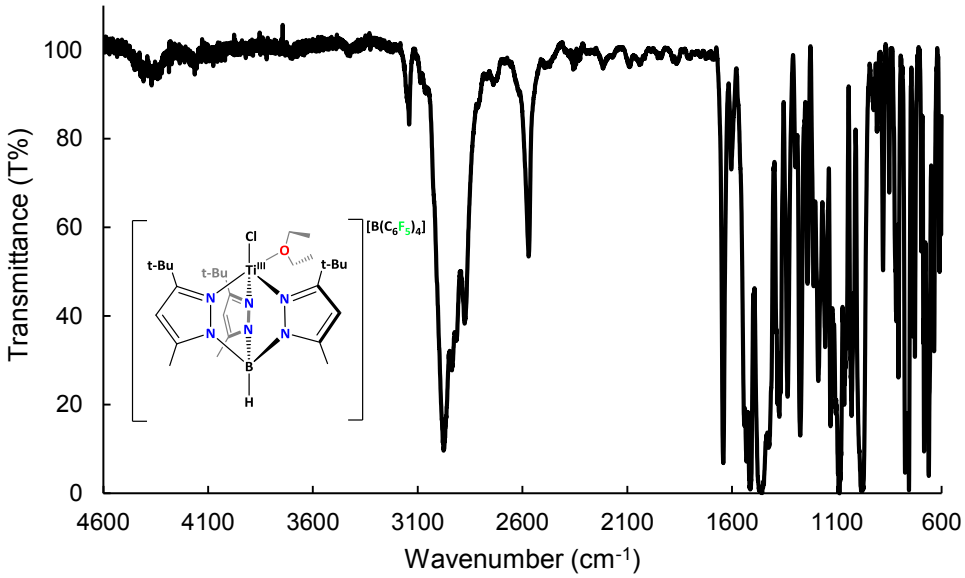

Figure S4.2.1: IR spectrum of solid $[(Tp^{tBu,Me})TiCl(OEt_2)][B(C_6F_5)_4]$, **3**, KBr pellet, cm^{-1}: υ = 2572 (B-H)

4.3 *IR Spectroscopy of [(Tp^{tBu,Me})Ti{≡NSi(CH$_3$)$_3$}(F)],* **4**

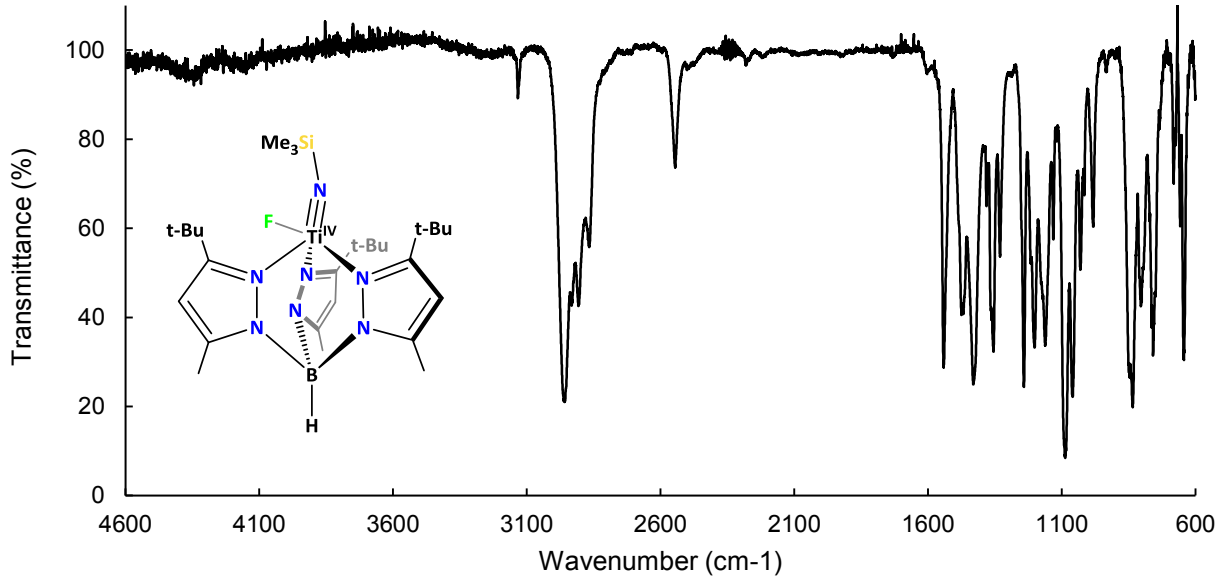

Figure S4.3.1: IR spectrum of solid [(Tp^{tBu,Me})Ti{≡NSi(CH$_3$)$_3$}(F)], **4**, KBr pellet, cm^{-1}: υ = 2545 (B-H)

5. UV-Vis Spectroscopy

5.1 *Concentrations from Figure 3 in Manuscript*

Compound Molecular Weight (g/mol)	Solvent	Solvent Density (g/mL)	Solvent (g)	Compound (mg)	Concentration (M)
2	Toluene	0.867	1.023	2.8	0.003763
2	THF	0.888	1.1748	3.2	0.003836
1	Toluene	0.867	0.8571	2.0	0.003406
1	THF	0.888	1.0513	2.7	0.00384
$\mathbf{3}^{\mathbf{Et_2O}}$	THF	0.888	1.4468	8.0	0.003897
$\mathbf{3}^{\mathbf{Et_2O}}$	Et_2O	0.713	1.7835	8.1	0.00257

Table S5.1.1: Concentrations and values for manuscript Figure 3 with respect to the electronic absorption spectra

5.2 *Electronic Absorption Spectroscopy of [(Tp^{tBu,Me})Ti{≡NSi(CH$_3$)$_3$}(THF)],* **2**

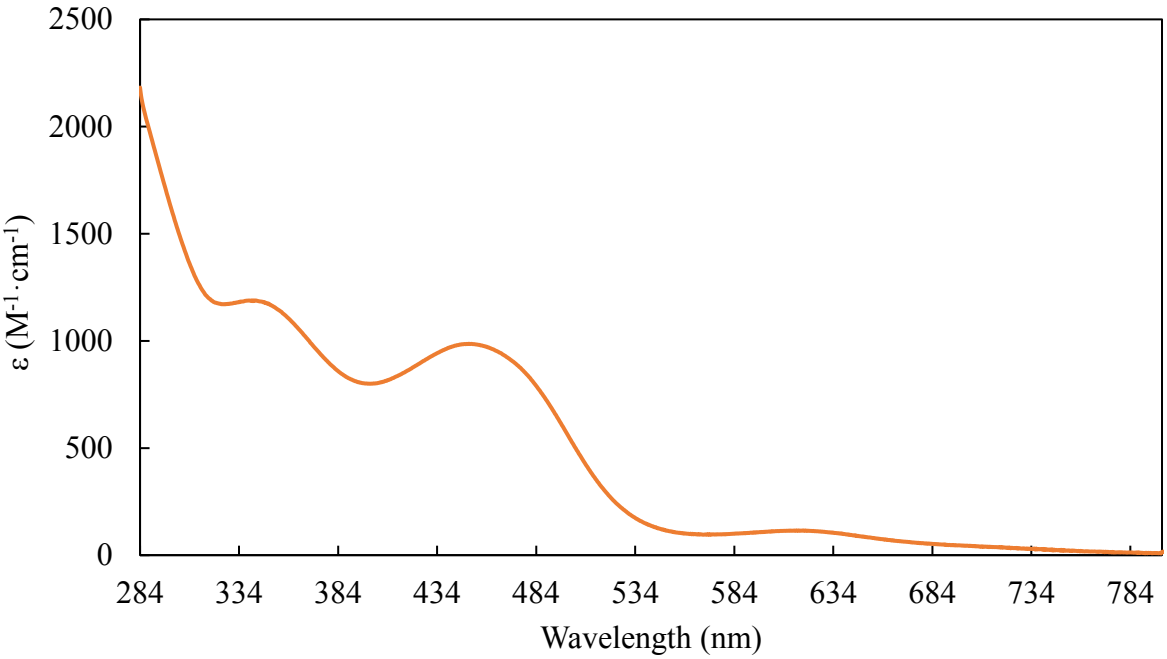

Figure S5.2.1: Electronic absorption spectrum of [(Tp^{tBu,Me})Ti{≡NSi(CH$_3$)$_3$}(THF)], **2**, in toluene (0.1314 mM). λ_{max} = 618nm, 453 nm, 344 nm

5.3 *Electronic Absorption Spectroscopy of [(Tp^{tBu,Me})TiCl(OEt$_2$)][B(C$_6$F$_5$)$_4$],* **3**

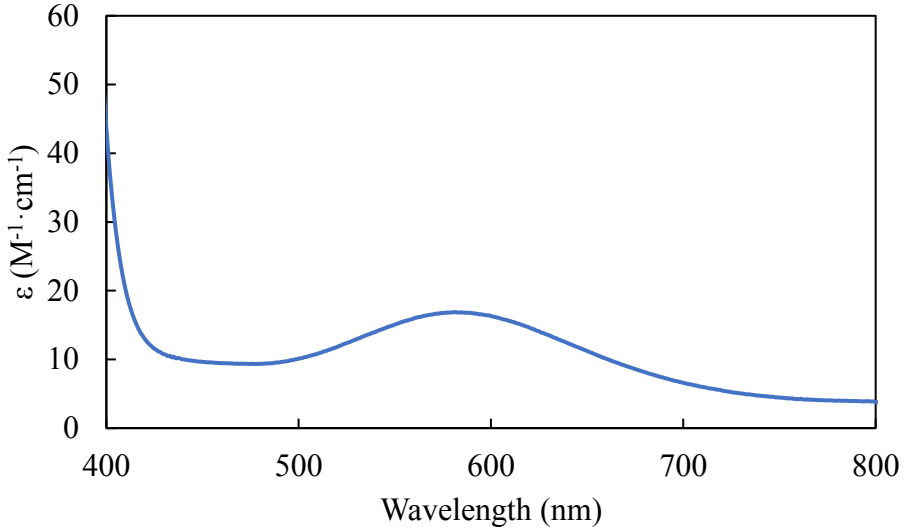

Figure S5.3.1: Electronic absorption spectrum of [(Tp^{tBu,Me})TiCl(OEt$_2$)][B(C$_6$F$_5$)$_4$], **3**, in THF (3.613 mM). λ_{max} = 574 nm

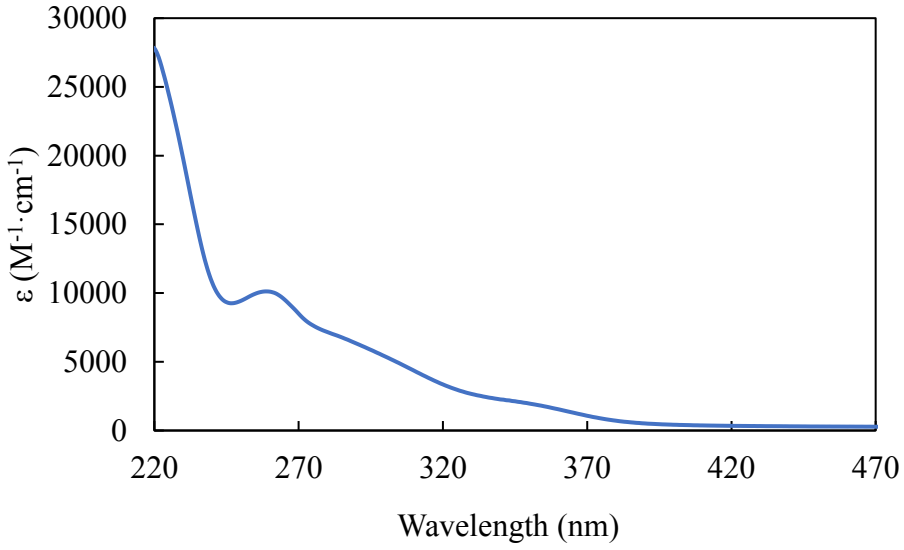

Figure S5.3.2: Electronic absorption spectrum of [(Tp^{tBu,Me})TiCl(OEt$_2$)][B(C$_6$F$_5$)$_4$], **3**, in THF (0.0425 mM). λ_{max} = 261 nm, 290 nm, 356 nm

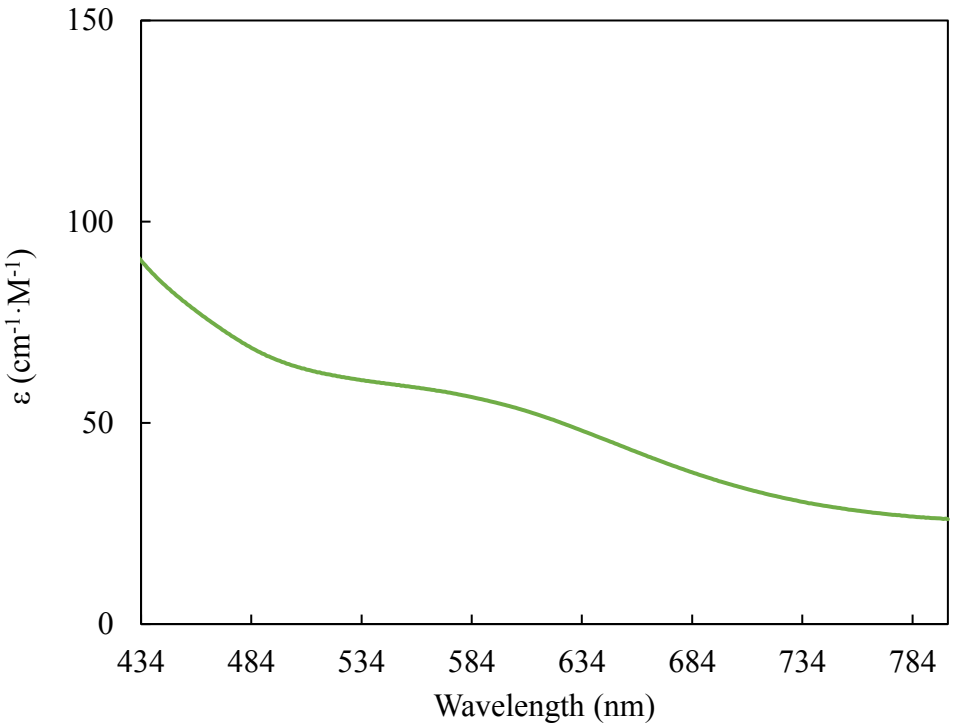

Figure S5.3.3: Electronic absorption spectrum in d-d transition wavelength range of [(Tp^{tBu,Me})TiCl(OEt$_2$)][B(C$_6$F$_5$)$_4$], **3**, in Et$_2$O (0.00257 mM). λ_{max} = 584 nm

5.4 *Electronic Absorption Spectroscopy of [(Tp^{tBu,Me})Ti{≡NSi(CH$_3$)$_3$)}(F)],* **4**

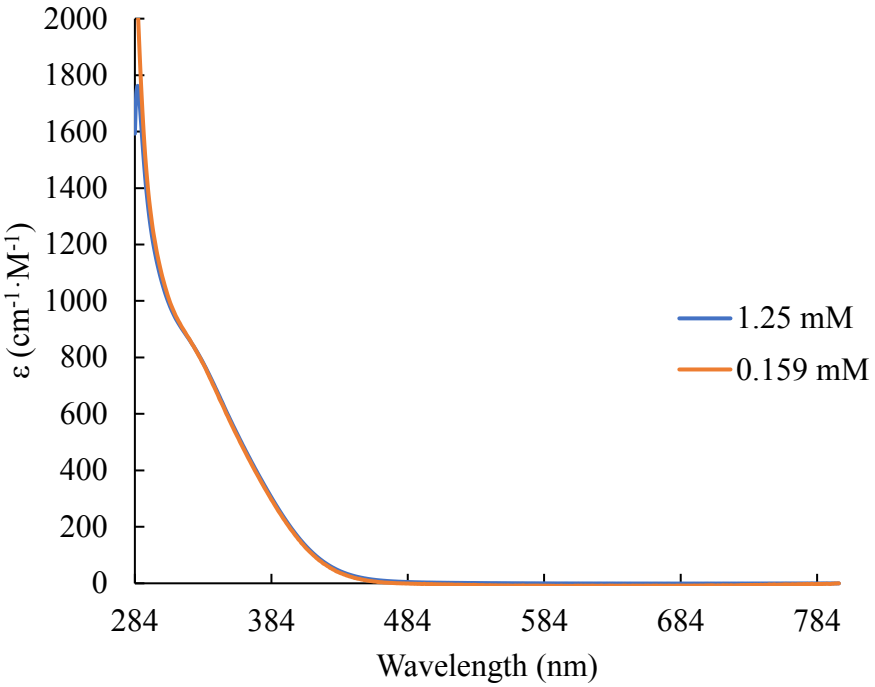

Figure S5.4.1: Electronic absorption spectrum of [(Tp^{tBu,Me})Ti{≡NSi(CH$_3$)$_3$)}(F)], **4**, in toluene (1.25 mM, blue trace and 0.159 mM, orange trace). λ_{max} = 328 nm

6. EPR Spectroscopy

6.1 *EPR Spectroscopy of [(Tp^{tBu,Me})Ti{≡NSi(CH$_3$)$_3$}(THF)],* ***2***

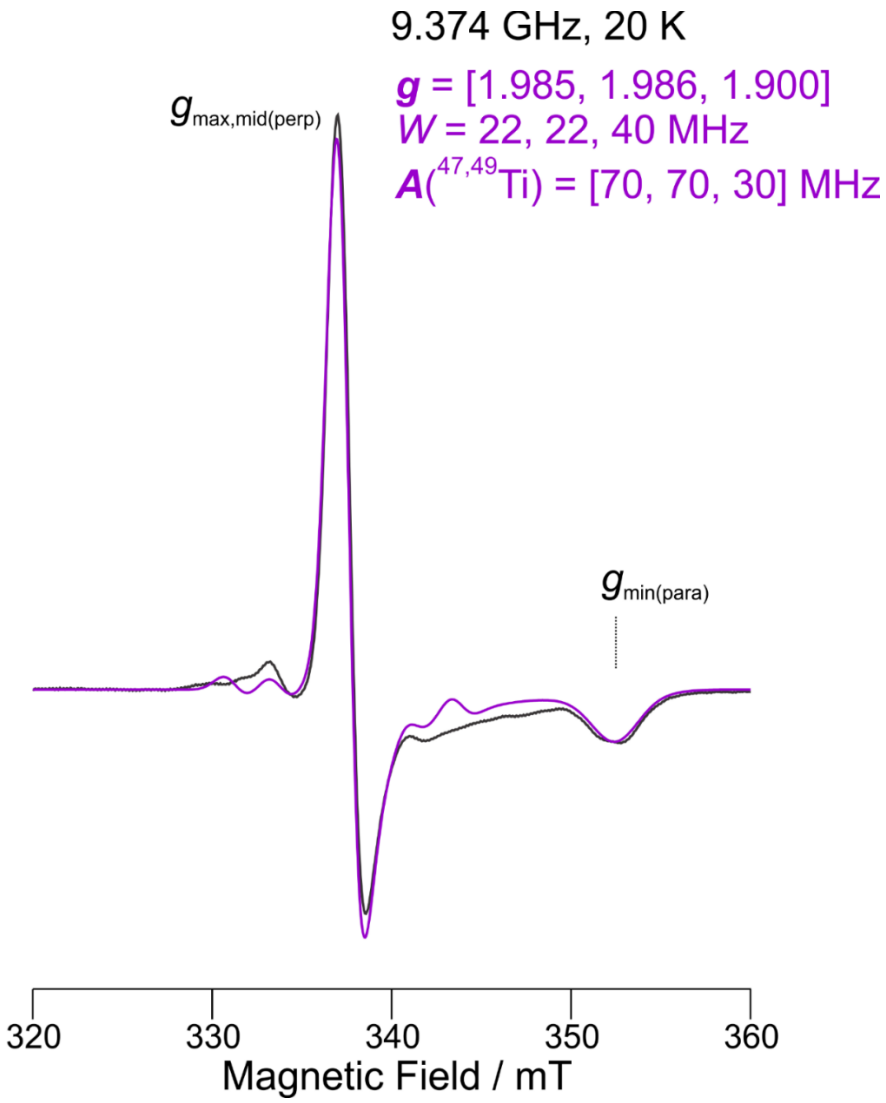

Figure S6.1.1: X-band EPR spectrum (as in Figure 3, main text) of **2** in 1:1 tol:THF glass showing an attempt to model the spectral satellites as arising from hyperfine coupling to $^{47,\ 49}$Ti (respectively, I = 5/2, 7.4% abundant and I = 7/2, 5.4% abundant). Because the g_N values for the two isotopes are within 0.01% of each other, the simulation simply used ^{47}Ti at 12.8% abundance, so that the outermost transitions involving m_I = ±7/2 are ignored. These are likely lost in the baseline in any case. The A values for ^{47,49}Ti are only rough estimates but demonstrate that the satellite features are of the proper intensity to arise from these magnetic nuclei. The main EPR features are from the three magnetically inactive nuclei, ^{46,48,50}Ti of which ^{48}Ti is 73.7% abundant. Quantitative analysis of ^{47,49}Ti hyperfine coupling typically requires single crystal studies, such as of Ti^{3+} sites in zircon.[24]

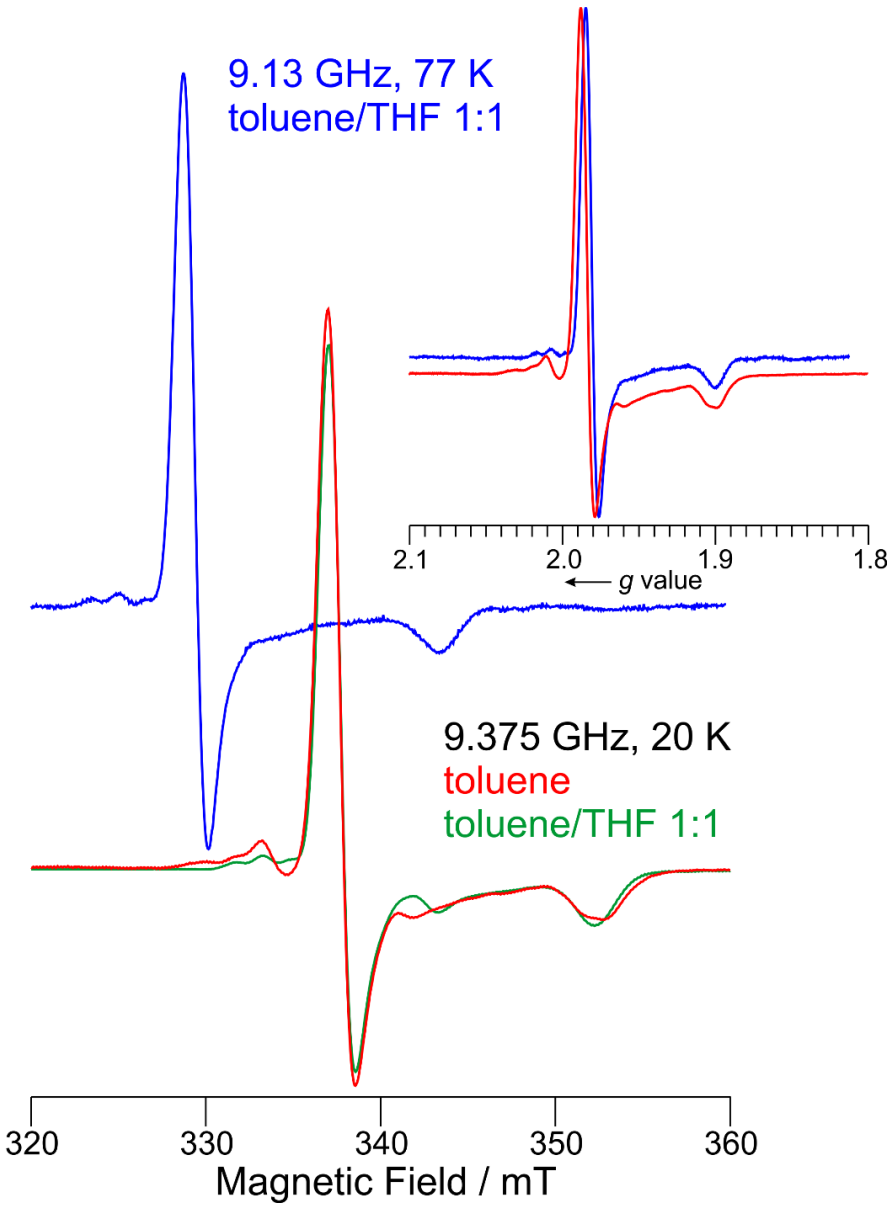

Figure S6.1.2: X-band EPR spectra of **2** showing the minimal effect of different solvents (note also that different preparations of **2** were used for each of the three spectra shown). The red and green traces were recorded on an EPR spectrometer equipped with an Oxford VT cryostat operating at 20 K and 9.375 GHz. The red trace is of **2** in neat toluene frozen solution; the green trace is in toluene/THF 1:1 (v/v) solution. The ^{47,49}Ti satellites' resolution is minimally different in these two solvents, but the major components are identical. The blue trace was also recorded in toluene/THF but on an EPR spectrometer equipped only with a finger dewar for liquid nitrogen, hence at 77 K and at 9.13 GHz (an analog frequency meter is used, rather than the higher precision digital meter used in the VT spectrometer). The inset displays the EPR spectra for the 20 K toluene and 77 K toluene/THF samples on a *g* value scale so that the difference in microwave frequency is removed and *g* values can be estimated as well. Despite the difference in spectrometer, sample preparation, temperature, and solvent, the spectra are identical within experimental variation.

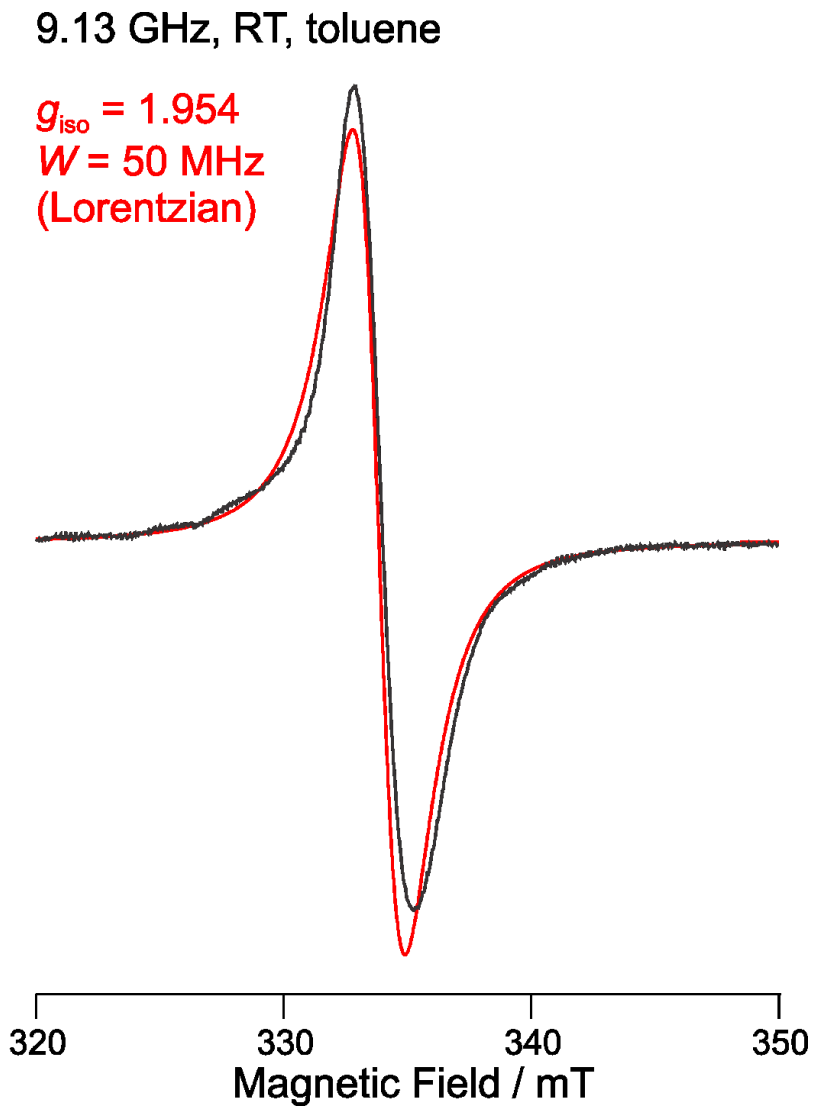

Figure S6.1.2: X-band EPR spectrum of **2** recorded at room temperature (black trace) with a simulation (red trace). No ^{47,49}Ti hyperfine coupling is resolved, in contrast to the X-band spectra in frozen solution (Fig. S6.1.1). The Lorentzian lineshape fits the experimental spectrum successfully which indicates that there is only a single species present in fluid solution (i.e., no inhomogeneous broadening). The isotropic g value, g_{iso} = 1.954, in fluid solution agrees with the average g value ($g_{ave} = g_x + g_y + g_z)/3$) in frozen solution ($g_{ave}$ = 1.957 at X-band; 1.961 at Q-band). Note that the room temperature X-band, low temperature X-band, and low temperature (absorption mode) Q-band spectra were recorded on three different spectrometers and are thus identical within experimental error. This correspondence indicates that the solution structure of **2** remains unchanged upon freezing.

6.2 *EPR Spectroscopy of [(Tp^{tBu,Me})TiCl(Solvent)][B(C$_6$F$_5$)$_4$],* **3^{Sol}**

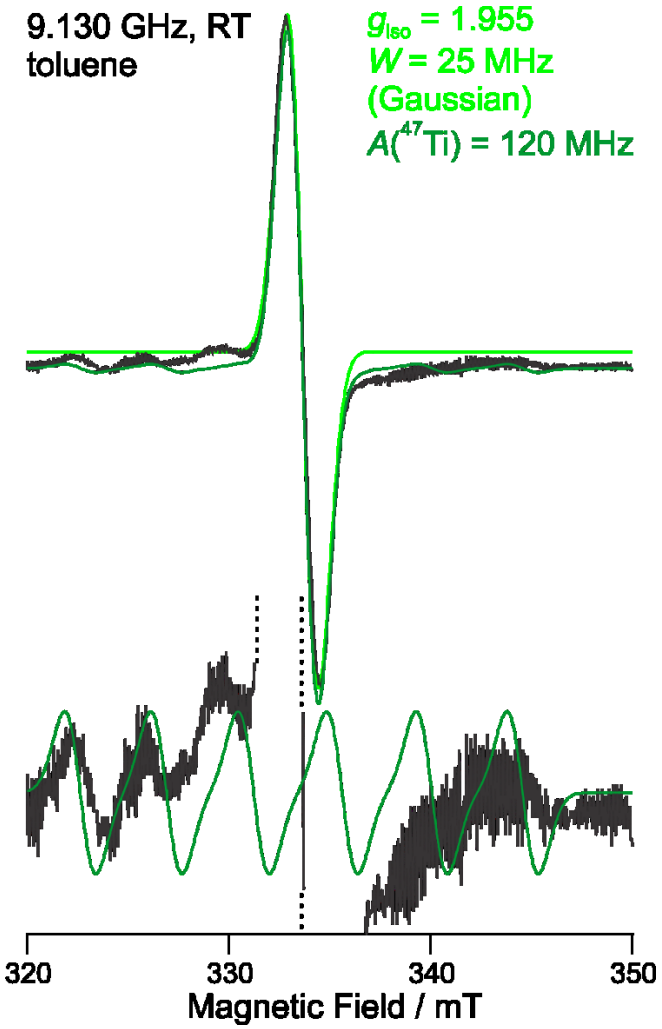

Figure S6.2.1: X-band EPR spectrum of **3^{Et_2O}** recorded in toluene solution at room temperature (black trace) with simulations (light green and dark green traces). The light green trace perfectly matches the experimental spectrum, with the narrow, but Gaussian, lineshape indicating that there is some inhomogeneous broadening. However, there are satellites not reproduced that are presumably due to ^{47,49}Ti hyperfine coupling. These are modelled in the dark green trace which includes A_{iso}(^{47}Ti) = 120 MHz in the appropriate isotopic weighting (12.8% abundance, as in Figure S6.1.1; ignoring the difference between ^{49}Ti and ^{47}Ti). The lower spectrum is a vertical expansion with the main (i.e., zero nuclear spin) experimental signal truncated. In this case, the simulation is of only ^{47}Ti and is simply scaled to match the satellite intensities. The isotropic g value, g_{iso} = 1.955, in fluid solution is close, but not identical to the average g value ($g_{ave} = g_x + g_y + g_z)/3$) = 1.933 in frozen solution determined at 35 GHz (Figure 3). This indicates that the fluid solution structure of **3** may become somewhat different upon freezing.

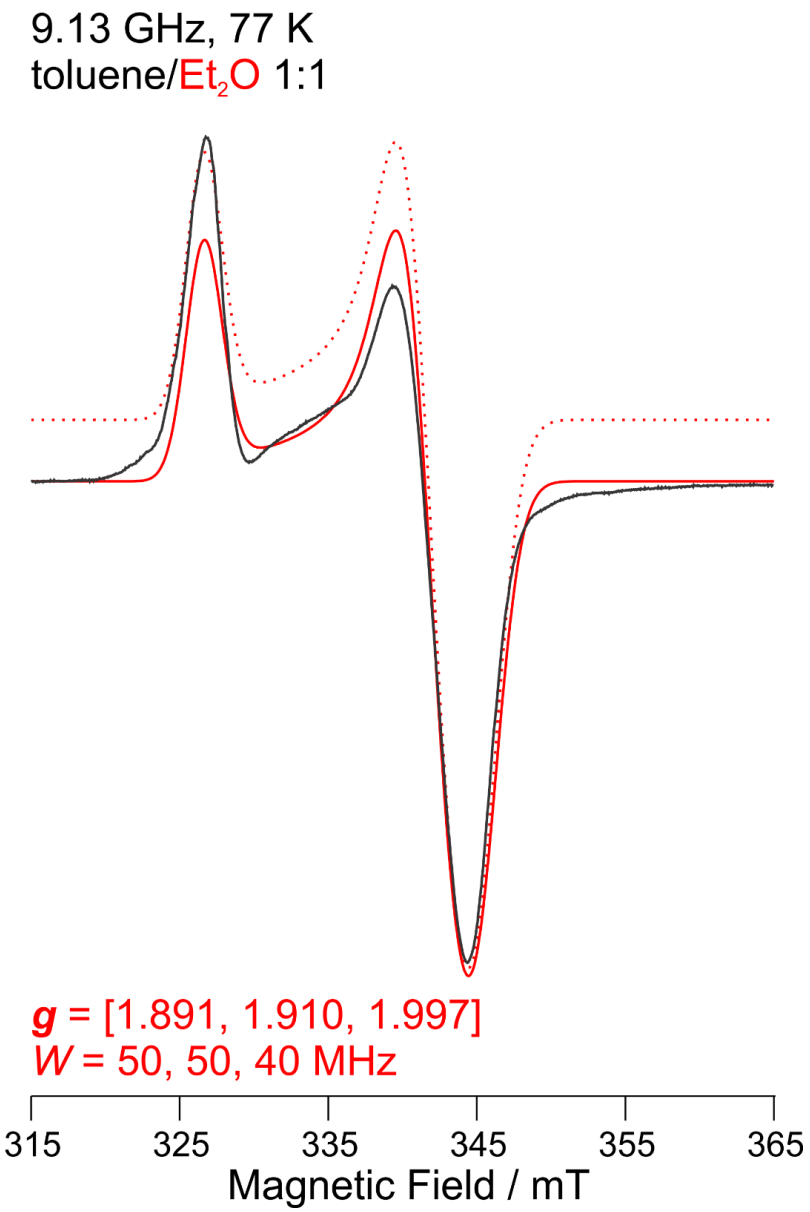

Figure S6.2.2: X-band EPR spectrum of $\mathbf{3}^{\mathbf{Et_2O}}$ recorded in toluene/Et_2O (1:1 v/v) solution at 77 K (black trace) with simulations (red traces; the dotted trace is offset to highlight the spectral match in the low field (high *g* value, parallel) region). The match is very close indicating that there is primarily a single species in toluene/Et_2O frozen solution. The slight discrepancies between experiment and simulation may be due to satellites from unresolved ^{47,49}Ti hyperfine coupling, particularly at the low field edge, but no attempt was made to model this effect. The average *g* value here, ($g_{ave} = g_x + g_y + g_z)/3) = 1.933, is identical to that in toluene solution at 35 GHz (Figure $\mathbf{3}^{\mathbf{Et_2O}}$, main text). This correspondence indicates that excess Et_2O has no effect on the frozen solution structure of $\mathbf{3}^{\mathbf{Et_2O}}$.

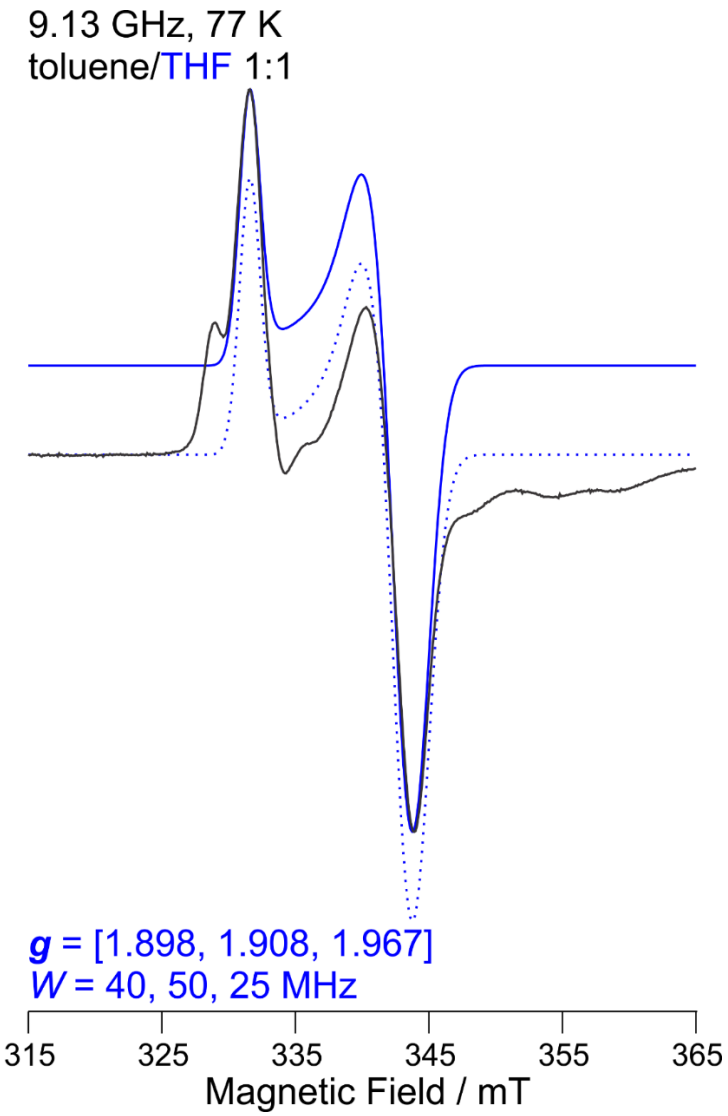

Figure S6.2.3: X-band EPR spectrum of $\mathbf{3^{Et_2O}}$ recorded in toluene/THF (1:1 v/v) solution at 77 K (black trace) with simulations (blue traces; the dotted trace is offset to highlight a spectral match to the baseline). The simulation reproduces a major species in toluene/THF frozen solution, but there are additional species that are not simulated and likely have a greater spread in g values, particularly towards low $g \approx 1.8$ (high field features at ~360 mT). The average g value even for the major (simulated) component, ($g_{ave} = g_x + g_y + g_z)/3) = 1.924$, is different from that in toluene solution at 35 GHz ($g_{ave} = 1.933$; Figure $\mathbf{3^{Et_2O}}$, main text). This indicates that excess THF does have an effect on the frozen solution structure, likely a solvent exchange.

7. Electrochemical Data

7.1 *Cyclic Voltammetry Studies of [(Tp^{tBu,Me})Ti{≡NSi(CH$_3$)$_3$}(Cl)],* **1**

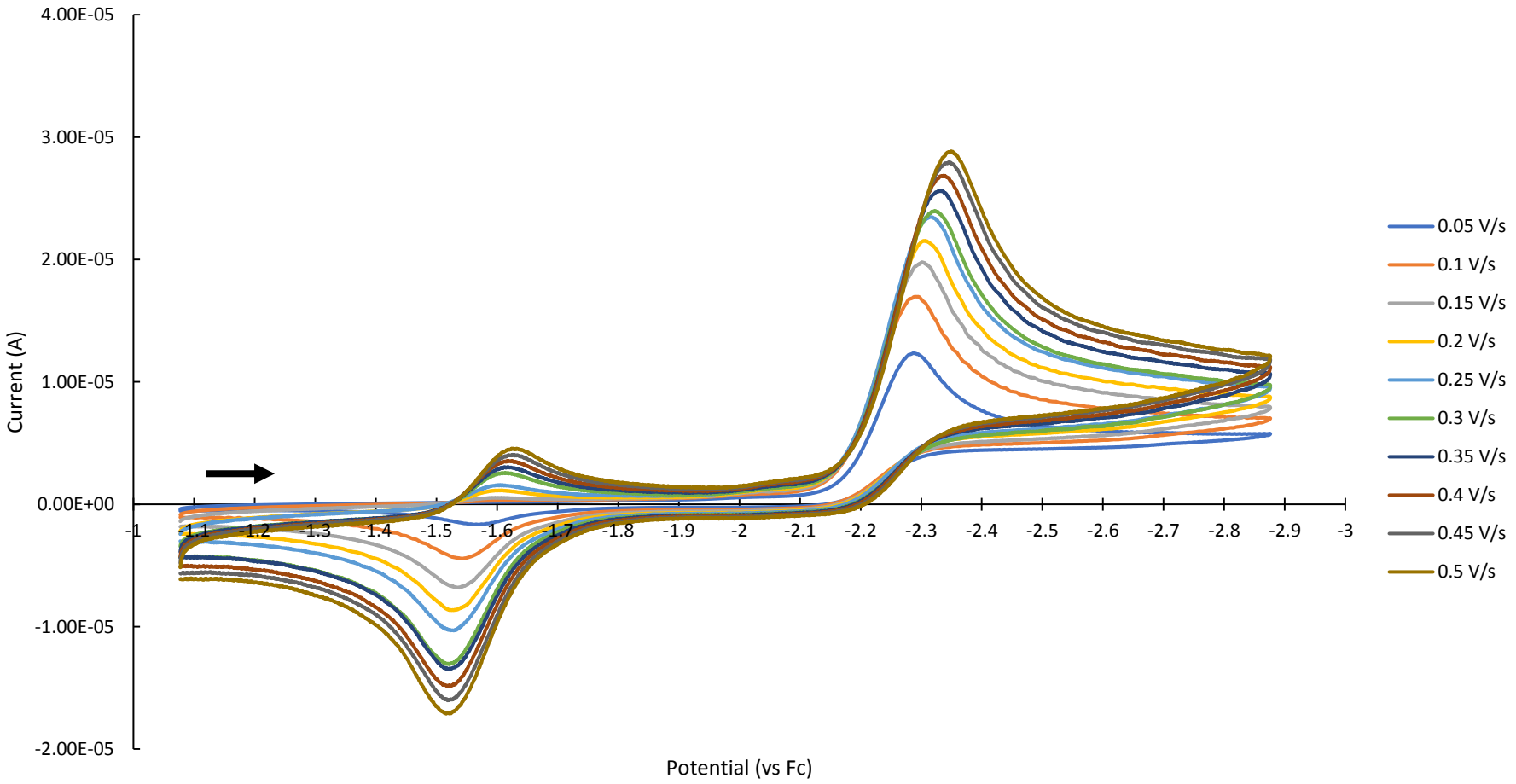

Figure S7.1.1: Cyclic voltammetry studies (CV) of [(Tp^{tBu,Me})Ti{≡NSi(CH$_3$)$_3$}(Cl)], **1**, (3.00 mM solution in THF) (negative scan starting from *ca.* -1.0 V) with 0.215 M supporting electrolyte [^{n}Bu$_4$N][PF$_6$] referenced to the FeCp$_2^{0/+}$ redox couple at 0.0 V (scan rate = 0.05-0.50 V/s).

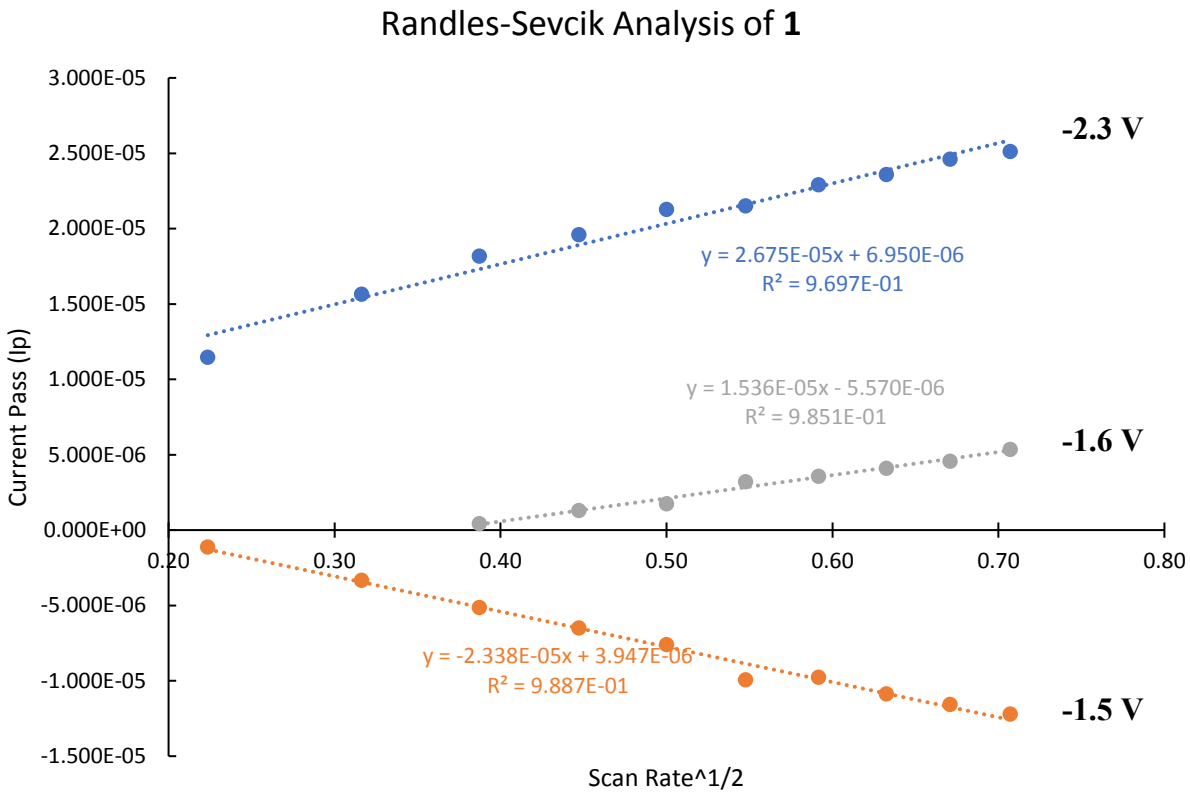

Figure S7.1.2: Randles-Sevcik analysis[10] of [(Tp^{tBu,Me})Ti{≡NSi(CH$_3$)$_3$}(Cl)], **1**, to show the lack of electrochemical reversibility of the reduction of **1** to **2**. Data sets are labeled with the potential of the corresponding electrochemical feature in Figure S7.1.1.

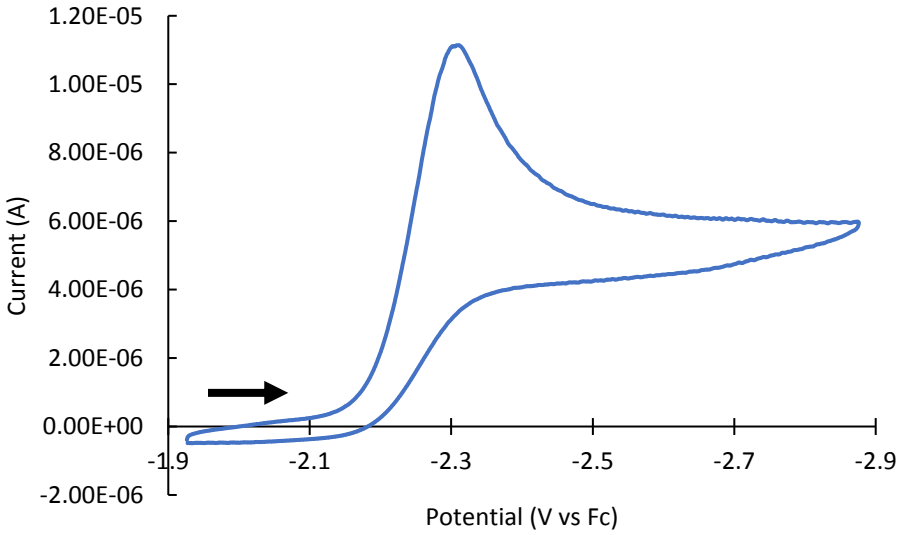

Figure S7.1.3: CV of irreversible reduction of [(Tp^{tBu,Me})Ti{≡NSi(CH$_3$)$_3$}(Cl)], **1**, isolated (scan window set to -1.93 to -2.78 V) at a scan rate of 0.1 V/s (3.00 mM solution in THF, negative scan starting from *ca.* -1.9 V with 0.215 M supporting electrolyte [^{n}Bu$_4$N][PF$_6$] referenced to the FeCp$_2^{0/+}$ redox couple at 0.0 V)

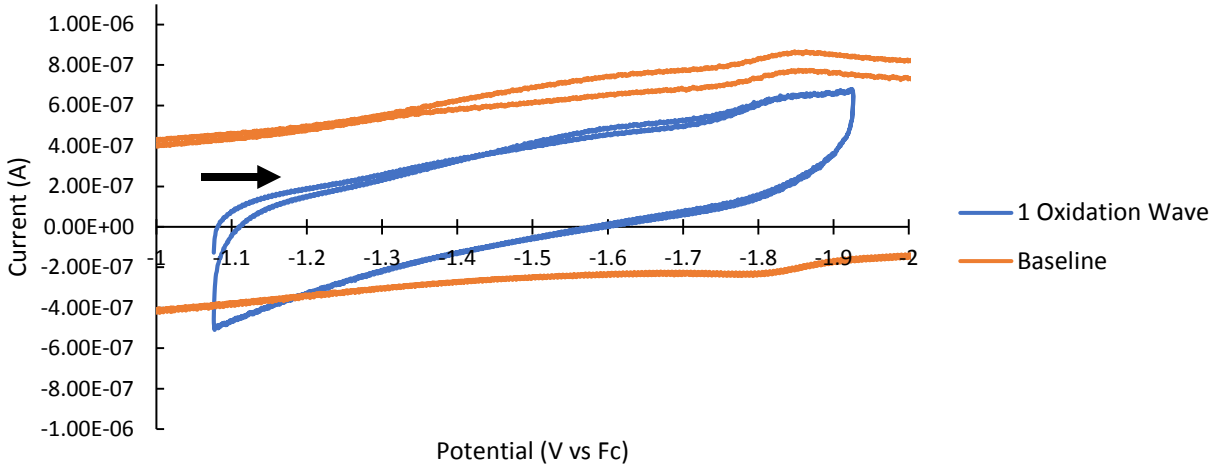

Figure S7.1.4: CV of [(Tp^{tBu,Me})Ti{≡NSi(CH$_3$)$_3$}(Cl)], **1**, isolated scan window (scan window of -1.076 to -1.926 V) showing the lack of Faradaic response in the region of the oxidation feature when not scanning to include reduction feature compared to the collected baseline. Scan rate = 0.1 V/s (3.00 mM solution in THF, negative scan starting from *ca.* -1.1 V with 0.215 M supporting electrolyte [^{n}Bu$_4$N][PF$_6$] referenced to the FeCp$_2^{0/+}$ redox couple at 0.0 V)

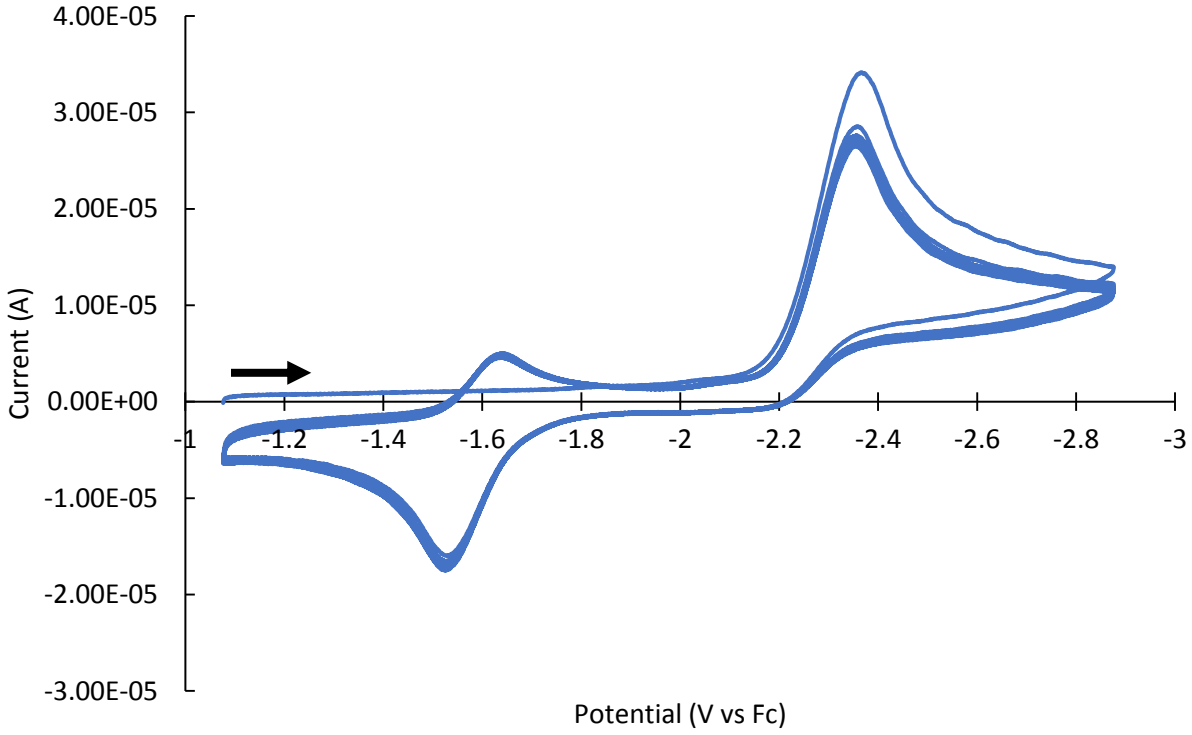

Figure S7.1.5: CV of [(Tp^{tBu,Me})Ti{≡NSi(CH$_3$)$_3$}(Cl)], **1**, shows no Faradaic response of the first reduction wave at -1.62 V when scanned before the latter reduction wave (-2.3 V) and shows stability over 40 sweeps (20 cycles) of the features. (3.00 mM solution in THF, negative scan starting from *ca.* -1.1 V with 0.215 M supporting electrolyte [^{n}Bu$_4$N][PF$_6$] referenced to the FeCp$_2^{0/+}$ redox couple at 0.0 V)

Tetrabutylammonium Chloride Addition				
Trial	**Amount (mg)**	**Moles (mmol)**	**Concentration (M)**	**Equivalents**
1	0	0.0000000	0.0000000	0.00
2	5.8	0.0208693	0.0030508	1.03
3	11.0	0.0395797	0.0057860	1.96
4	16.8	0.0604491	0.0088368	2.99
5	22.5	0.0809585	0.0118350	4.01

Table S7.1.6: Addition of [^{n}Bu$_4$N][Cl] to CV experiment of **1.**. This experiment for the addition of chloride was set up identically to that of S7.1.1, however after scans were taken at each scan rate at a given concentration of chloride ions in solution, more chloride was added (the difference between each trial; *e.g.* for trial 3, an additional 5.2 mg of chloride was added for a total of 11 mg of chloride in solution) and the current response at each scan rate was measured again.

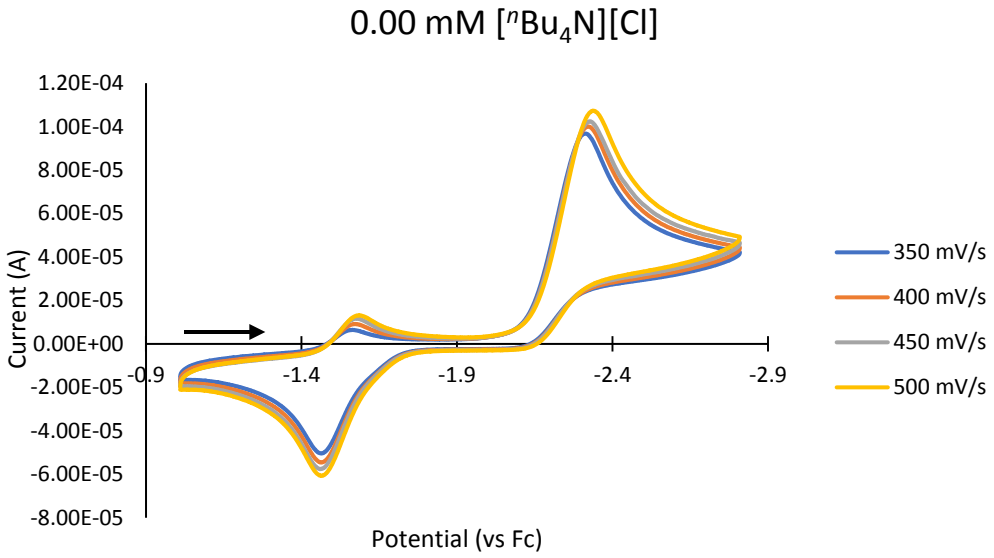

Figure S7.1.7: Cyclic voltammetry studies (CV) of [(Tp^{tBu,Me})Ti{≡NSi(CH$_3$)$_3$}(Cl)], **1**, (2.95 mM solution in THF) (negative scan starting from *ca.* -1.0 V) with 0.204 M supporting electrolyte [nBu$_4$N][PF$_6$] referenced to the FeCp$_2^{0/+}$ redox couple at 0.0 V (scan rate = 0.35-0.50 V/s) and no addition of chloride.

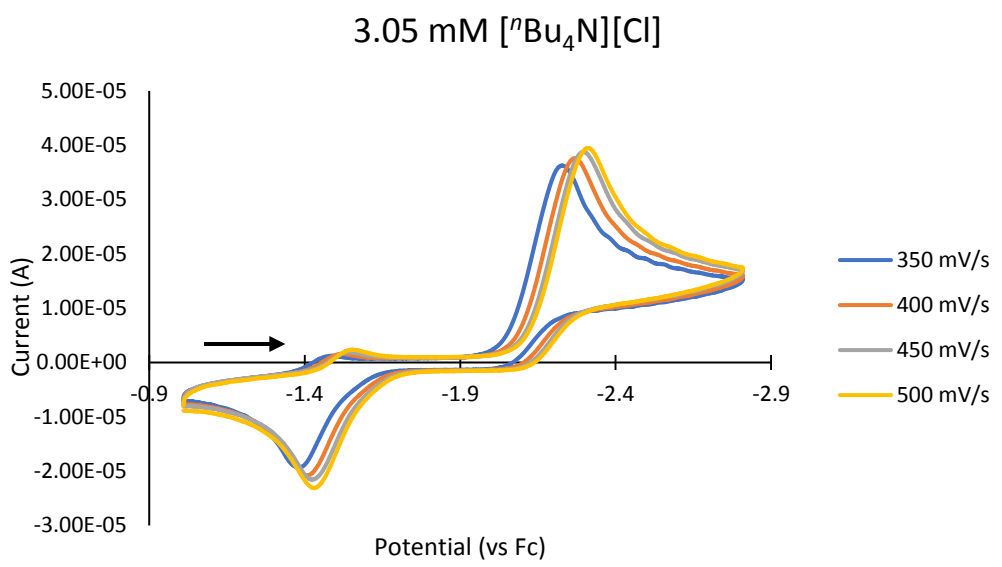

Figure S7.1.8: Cyclic voltammetry studies (CV) of [(Tp^{tBu,Me})Ti{≡NSi(CH$_3$)$_3$}(Cl)], **1**, (2.95 mM solution in THF) and [^{n}Bu$_4$N][Cl] (3.05 mM) (negative scan starting from *ca.* -1.0 V) with 0.204 M supporting electrolyte [^{n}Bu$_4$N][PF$_6$] referenced to the FeCp$_2^{0/+}$ redox couple at 0.0 V (scan rate = 0.35-0.50 V/s). Quasi-reversible event at *ca.* -1.6 V has begun to disappear.

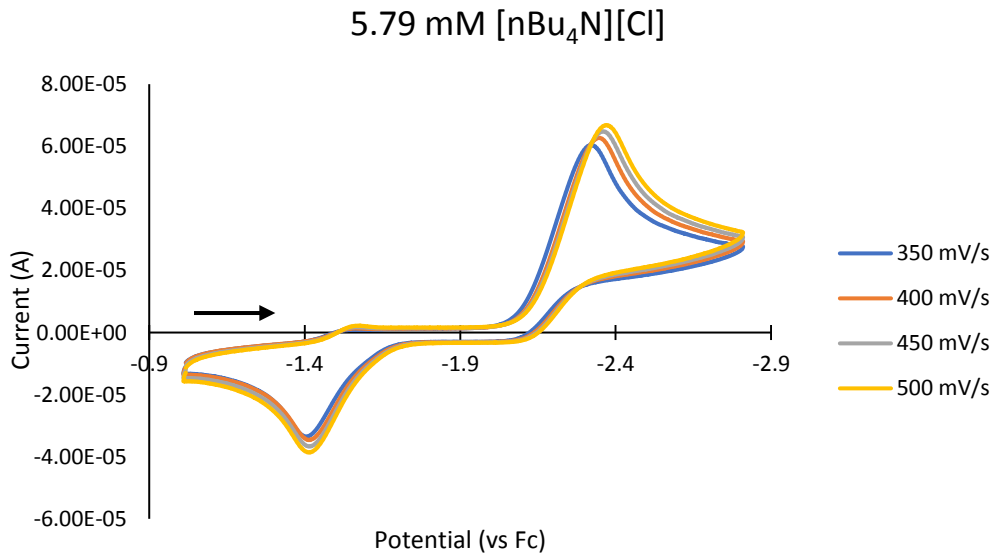

Figure S7.1.9: Cyclic voltammetry studies (CV) of [(Tp^{tBu,Me})Ti{≡NSi(CH$_3$)$_3$}(Cl)], **1**, (2.95 mM solution in THF) and [^{n}Bu$_4$N][Cl] (5.79 mM) (negative scan starting from *ca.* -1.0 V) with 0.204 M supporting electrolyte [^{n}Bu$_4$N][PF$_6$] referenced to the FeCp$_2^{0/+}$ redox couple at 0.0 V (scan rate = 0.35-0.50 V/s). Quasi-reversible event at *ca.* -1.6 V has virtually disappeared.

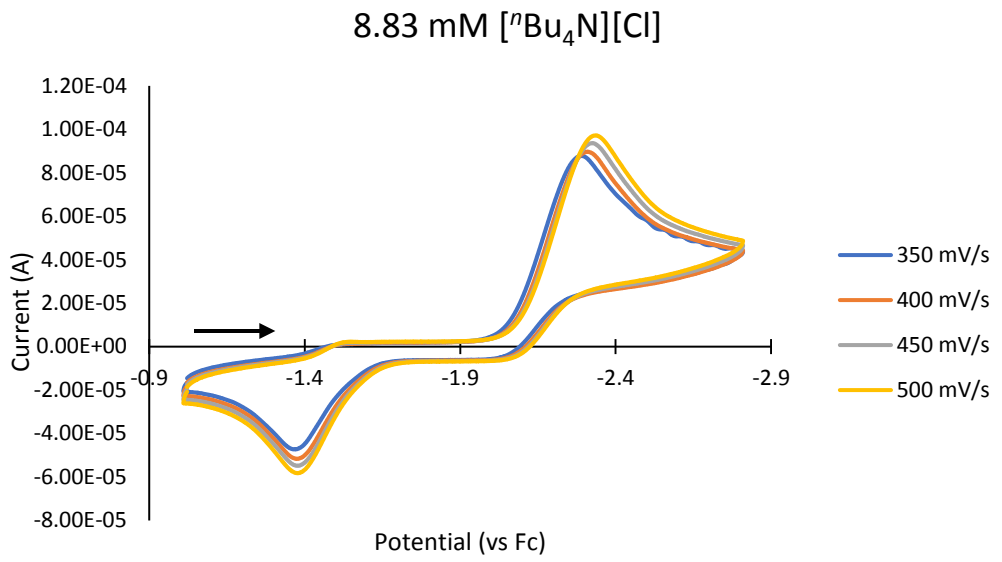

Figure S7.1.10: Cyclic voltammetry studies (CV) of [(Tp^{tBu,Me})Ti{≡NSi(CH$_3$)$_3$}(Cl)], **1**, (2.95 mM solution in THF) and [^{n}Bu$_4$N][Cl] (8.83 mM) (negative scan starting from *ca.* -1.0 V) with 0.204 M supporting electrolyte [^{n}Bu$_4$N][PF$_6$] referenced to the FeCp$_2^{0/+}$ redox couple at 0.0 V (scan rate = 0.35-0.50 V/s). Quasi-reversible event at ca. -1.6 V has disappeared.

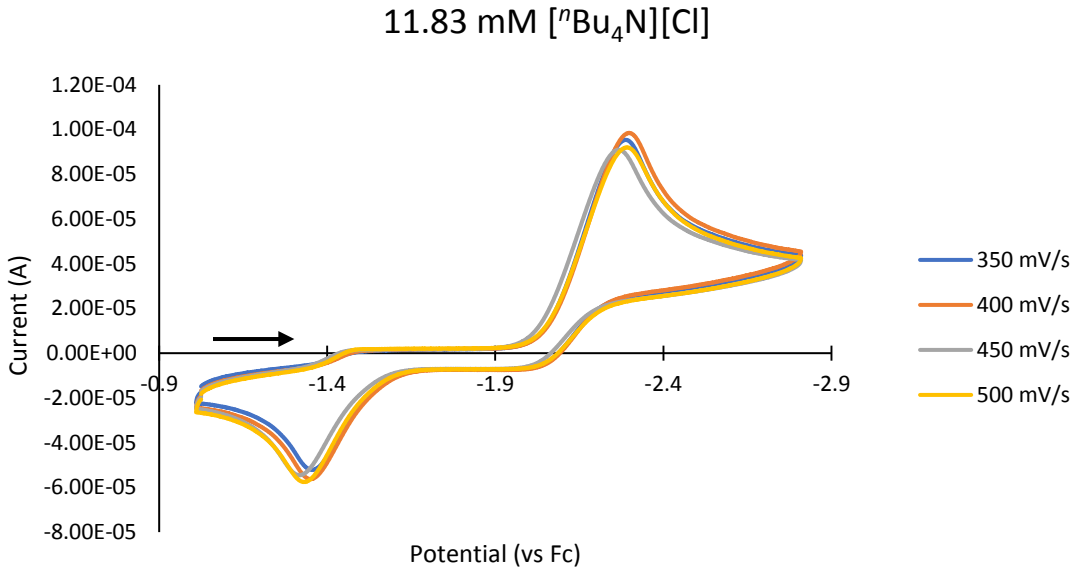

Figure S7.1.11: Cyclic voltammetry studies (CV) of [(Tp^{tBu,Me})Ti{≡NSi(CH$_3$)$_3$}(Cl)], **1**, (2.95 mM solution in THF) and [^{n}Bu$_4$N][Cl] (11.83 mM) (negative scan starting from *ca.* -1.0 V) with 0.204 M supporting electrolyte [^{n}Bu$_4$N][PF$_6$] referenced to the FeCp$_2^{0/+}$ redox couple at 0.0 V (scan rate = 0.35-0.50 V/s). Quasi-reversible event at ca. -1.6 V has disappeared.

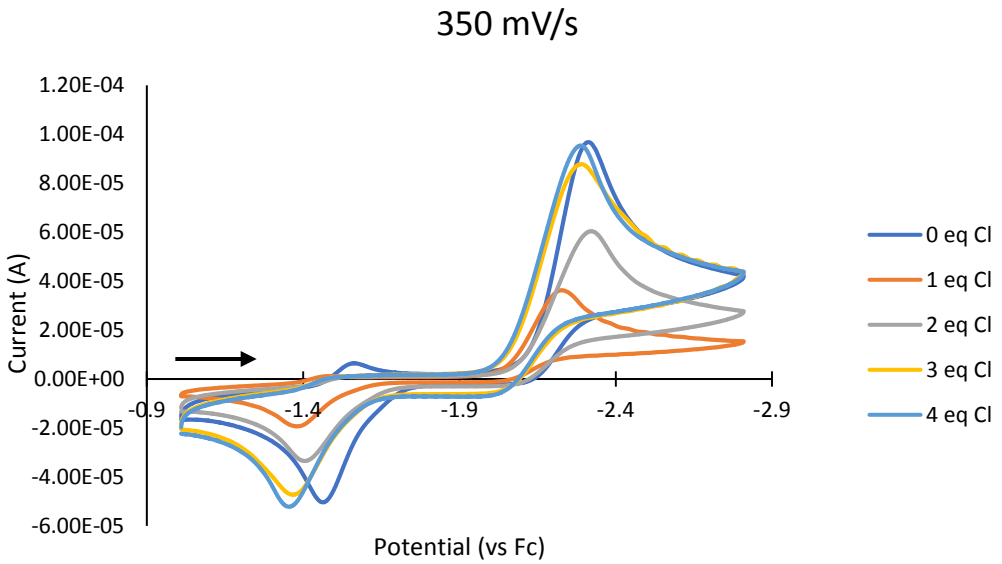

Figure S7.1.12: Cyclic voltammetry studies (CV) of [(Tp^{tBu,Me})Ti{≡NSi(CH$_3$)$_3$}(Cl)], **1**, (2.95 mM solution in THF) (negative scan starting from *ca.* -1.0 V) with 0.204 M supporting electrolyte [^{n}Bu$_4$N][PF$_6$] referenced to the FeCp$_2^{0/+}$ redox couple at 0.0 V. Shown at a constant scan rate (350 mV/s) dependent on chloride concentration. The shift in the potential for the oxidation event suggests that the chloride complex is slightly more oxidizing than the average of [(Tp^{tBu,Me})Ti{≡NSi(CH$_3$)$_3$}(Cl)]$^{0/-}$ and [(Tp^{tBu,Me})Ti{≡NSi(CH$_3$)$_3$}(THF)]$^{+/0}$ complexes (shown at zero equivalents of chloride in dark blue). This also shows the loss of the quasi-reversibility of the proposed [(Tp^{tBu,Me})Ti{≡NSi(CH$_3$)$_3$}(THF)]$^{+/0}$ redox event at *ca.* -1.6 V after just one equivalent of chloride added to the electrochemical cell.

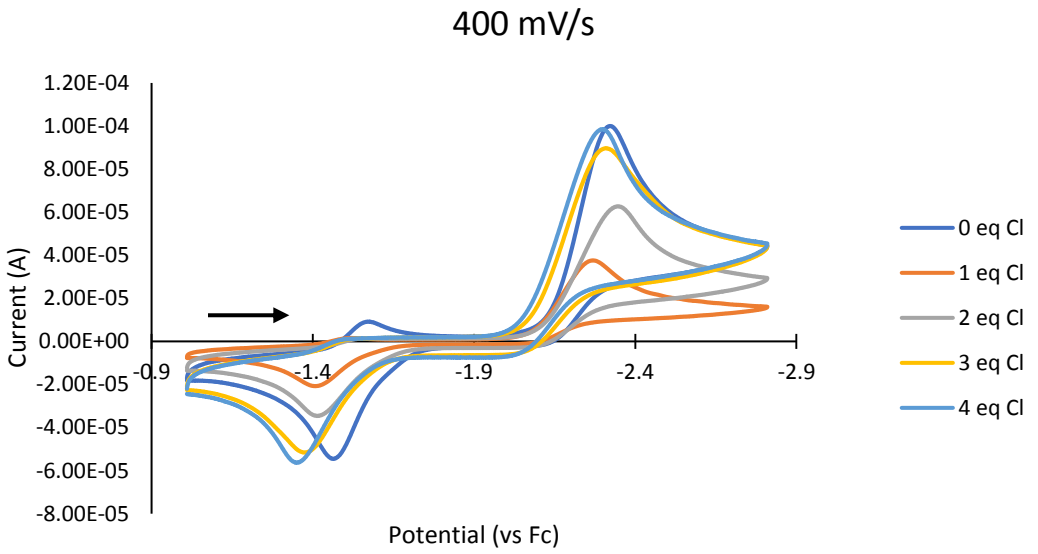

Figure S7.1.13: Cyclic voltammetry studies (CV) of [(Tp^{tBu,Me})Ti{≡NSi(CH$_3$)$_3$}(Cl)], **1**, (2.95 mM solution in THF) (negative scan starting from *ca.* -1.0 V) with 0.204 M supporting electrolyte [^{n}Bu$_4$N][PF$_6$] referenced to the FeCp$_2^{0/+}$ redox couple at 0.0 V. Shown at a constant scan rate (400 mV/s) dependent on chloride concentration. The shift in the potential for the oxidation event suggests that the chloride complex is slightly more oxidizing than the average of [(Tp^{tBu,Me})Ti{≡NSi(CH$_3$)$_3$}(Cl)]$^{0/-}$ and [(Tp^{tBu,Me})Ti{≡NSi(CH$_3$)$_3$}(THF)]$^{+/0}$ salts (shown at zero equivalents of chloride in dark blue). This also shows the loss of the quasi-reversibility of the proposed [(Tp^{tBu,Me})Ti{≡NSi(CH$_3$)$_3$}(THF)]$^{+/0}$ redox event at *ca.* -1.6 V after just one equivalent of chloride added to the electrochemical cell.

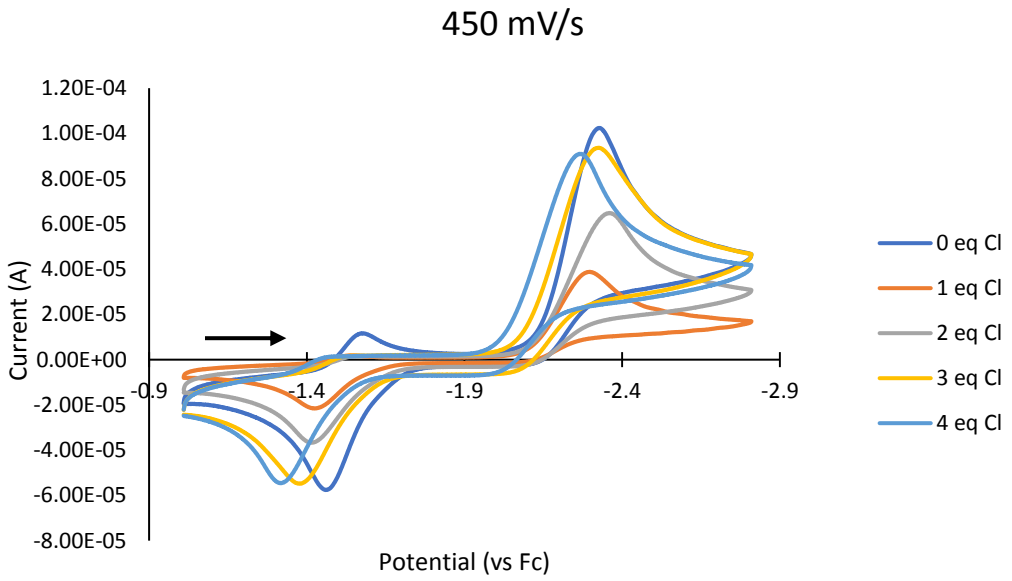

Figure S7.1.14: Cyclic voltammetry studies (CV) of [(Tp^{tBu,Me})Ti{≡NSi(CH$_3$)$_3$}(Cl)], **1**, (2.95 mM solution in THF) (negative scan starting from *ca.* -1.0 V) with 0.204 M supporting electrolyte [^{n}Bu$_4$N][PF$_6$] referenced to the FeCp$_2^{0/+}$ redox couple at 0.0 V. Shown at a constant scan rate (450 mV/s) dependent on chloride concentration. The shift in the potential for the oxidation event suggests that the chloride complex is slightly more oxidizing than the average of [(Tp^{tBu,Me})Ti{≡NSi(CH$_3$)$_3$}(Cl)]$^{0/-}$ and [(Tp^{tBu,Me})Ti{≡NSi(CH$_3$)$_3$}(THF)]$^{+/0}$ complexes (shown at zero equivalents of chloride in dark blue). This also shows the loss of the quasi-reversibility of the proposed [(Tp^{tBu,Me})Ti{≡NSi(CH$_3$)$_3$}(THF)]$^{+/0}$ redox event at *ca.* -1.6 V after just one equivalent of chloride added to the electrochemical cell.

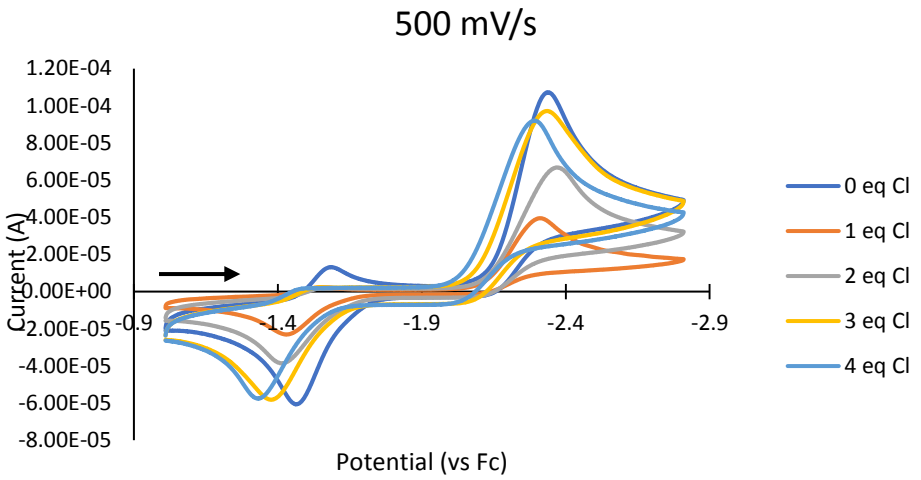

Figure S7.1.15: Cyclic voltammetry studies (CV) of [(Tp^{tBu,Me})Ti{≡NSi(CH$_3$)$_3$}(Cl)], **1**, (2.95 mM solution in THF) (negative scan starting from *ca.* -1.0 V) with 0.204 M supporting electrolyte [^{n}Bu$_4$N][PF$_6$] referenced to the FeCp$_2^{0/+}$ redox couple at 0.0 V. Shown at a constant scan rate (500 mV/s) dependent on chloride concentration. The shift in the potential for the oxidation event suggests that the chloride complex is slightly more oxidizing than the average of [(Tp^{tBu,Me})Ti{≡NSi(CH$_3$)$_3$}(Cl)]$^{0/-}$ and [(Tp^{tBu,Me})Ti{≡NSi(CH$_3$)$_3$}(THF)]$^{+/0}$ salts (shown at zero equivalents of chloride in dark blue). This also shows the loss of the quasi-reversibility of the proposed [(Tp^{tBu,Me})Ti{≡NSi(CH$_3$)$_3$}(THF)]$^{+/0}$ redox event at *ca.* -1.6 V after just one equivalent of chloride added to the electrochemical cell.

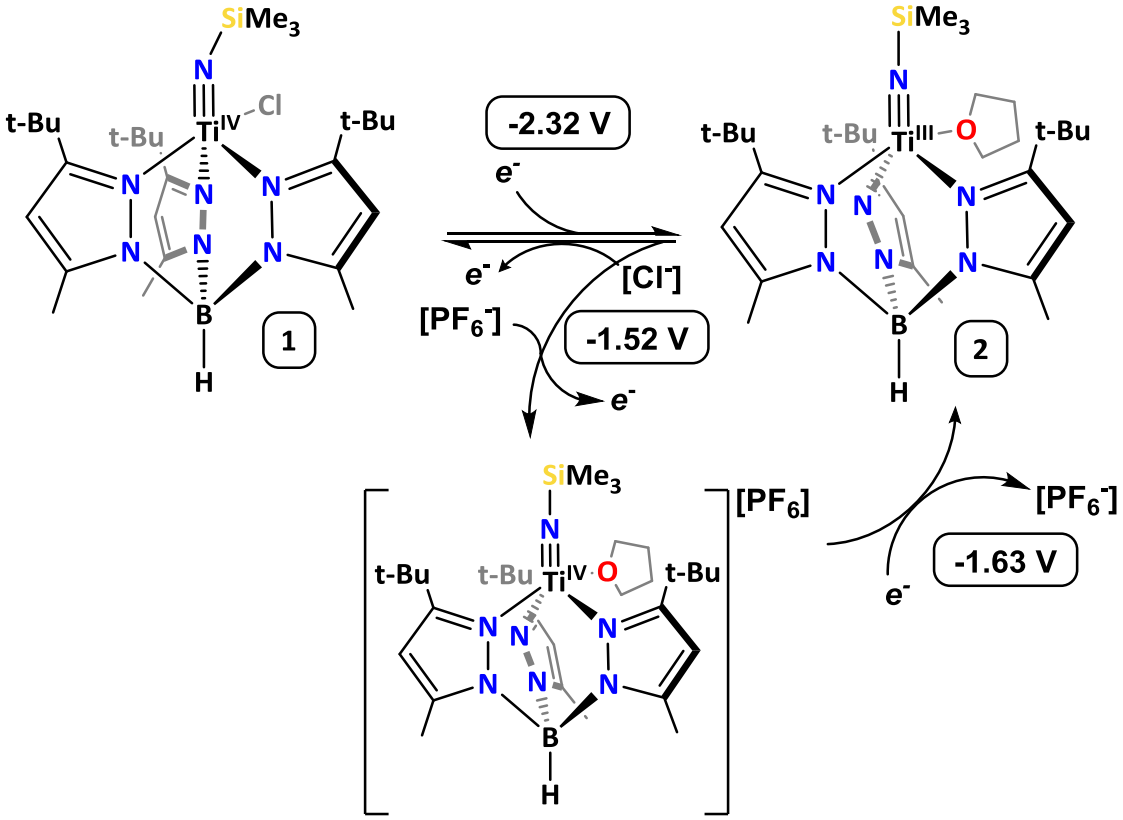

Figure S7.1.16: Proposed electrochemical mechanism for **1**. This helps to explain that at relatively low concentrations of chloride in solution, the proposed $Ti^{IV}[PF_6]$ salt forms. This can be prevented by the addition of chloride to the electrochemical cell. The redox events are also slightly shifted when chloride concentration is relatively high from *ca.* -1.45 V to -1.35 V (at scan rates ≥300 mV/s) indicating that the chloride salt is slightly more oxidizing than the $[PF_6]$ salt.

7.2 *Cyclic Voltammetry Studies of [(Tp^{tBu,Me})Ti{≡NSi(CH$_3$)$_3$}(THF)],* **2**

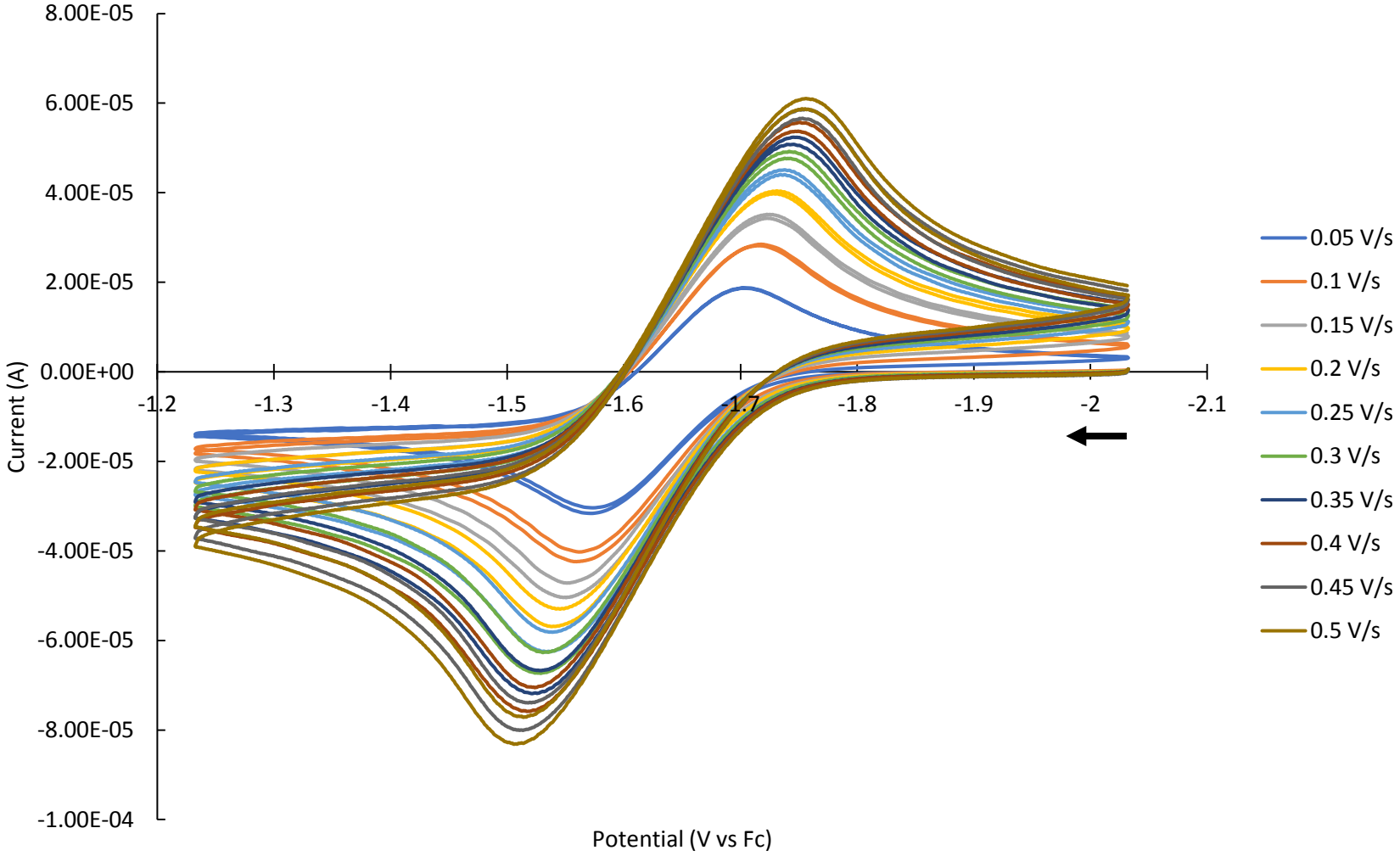

Figure S7.2.1: Cyclic voltammetry studies (CV) of [(Tp^{tBu,Me})Ti{≡NSi(CH$_3$)$_3$}(THF)], **2** (3.39 mM solution in THF) (positive scan starting at *ca.* -2 V) with 0.271 M supporting electrolyte [^{n}Bu$_4$N][PF$_6$] referenced to the FeCp$_2^{0/+}$ redox couple at 0.0 V (scan rate = 0.05-0.50 V/s).

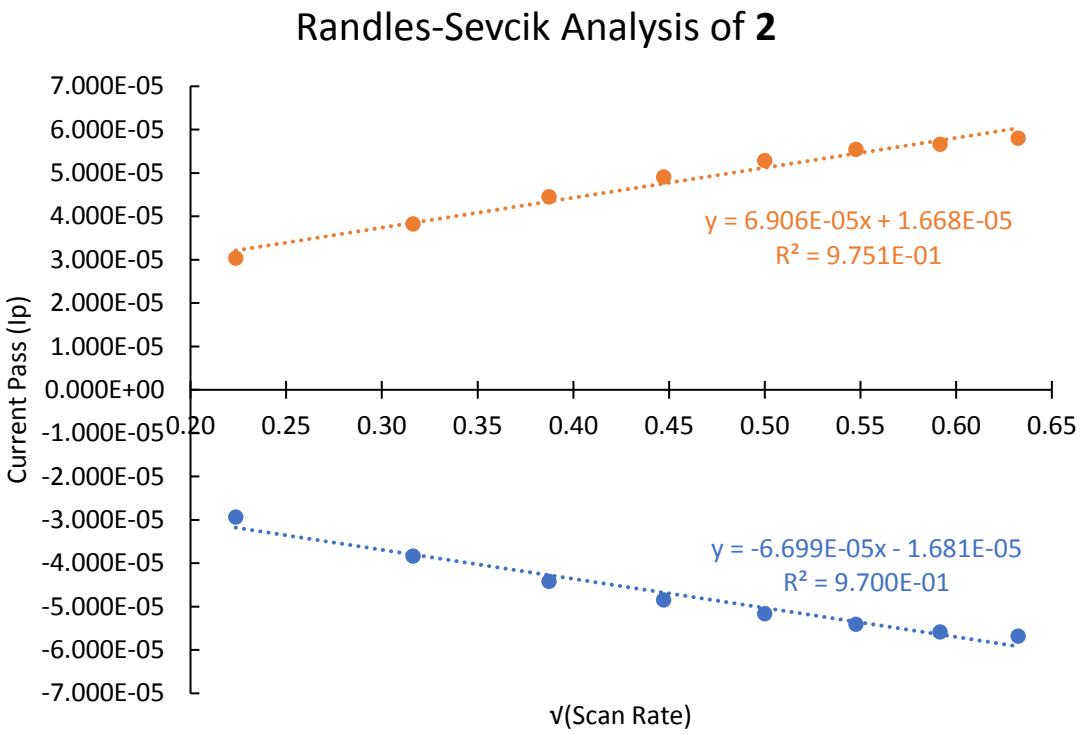

Figure S7.2.2: Randles-Sevcik analysis[10] of [(Tp^{tBu,Me})Ti{≡NSi(CH$_3$)$_3$}(THF)], **2**, to illustrate the electrochemical reversibility of the oxidation/reduction of **2**.

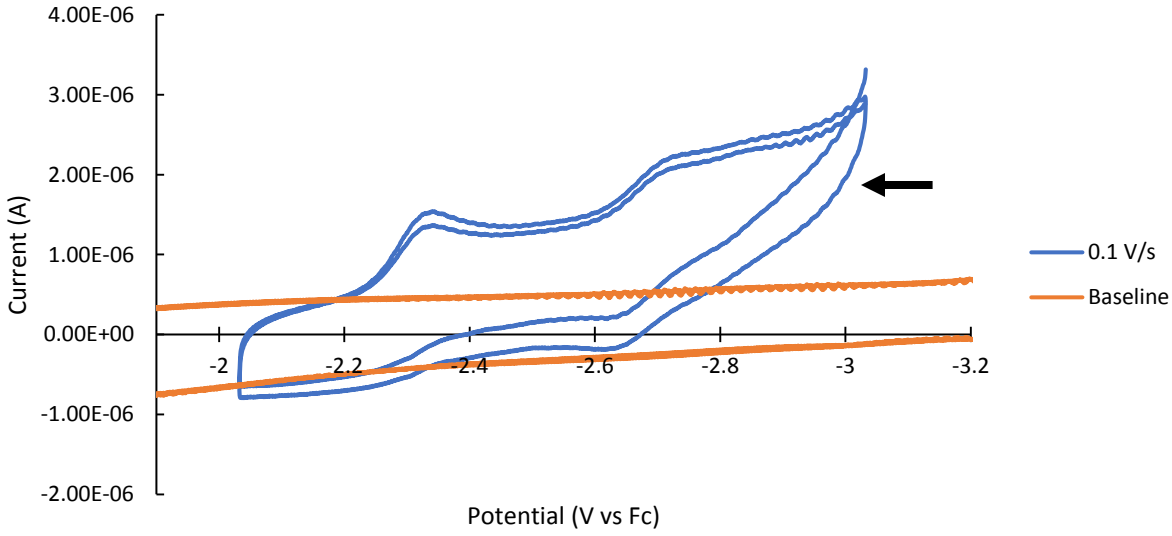

Figure S7.2.3: CV of small impurity present in [(Tp^{tBu,Me})Ti{≡NSi(CH$_3$)$_3$}(THF)], **2**, compared to the collected baseline with one order of magnitude less current response compared to **2** (3.39 mM solution in THF) (positive scan starting at *ca.* -2 V) with 0.271 M supporting electrolyte [^{n}Bu$_4$N][PF$_6$] referenced to the $FeCp_2^{0/+}$ redox couple at 0.0 V.

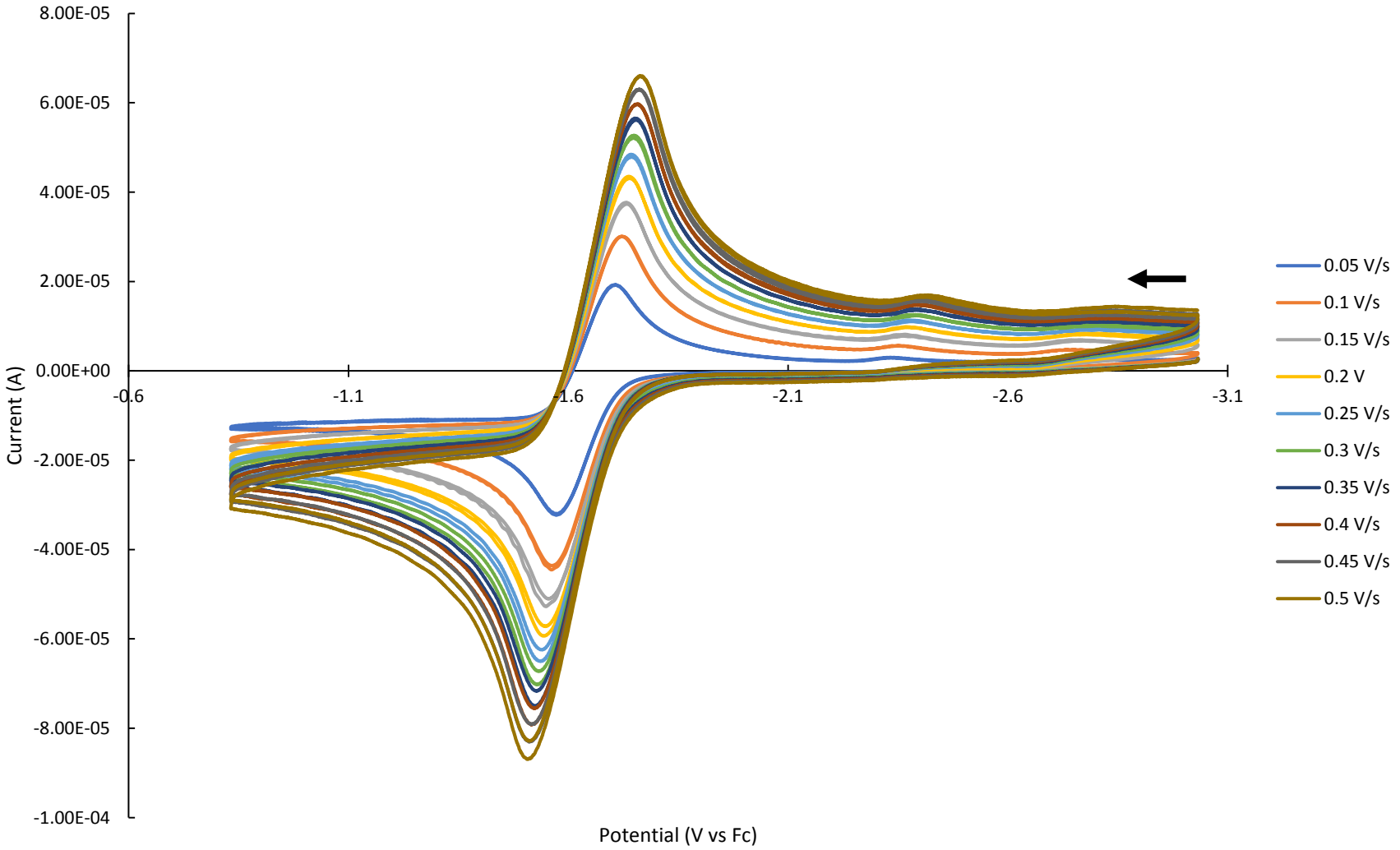

Figure S7.2.4: CV of [(Tp^{tBu,Me})Ti{≡NSi(CH$_3$)$_3$}(THF)], **2**, (3.39 mM solution in THF) (positive scan starting at *ca.* -2.9 V) with 0.271 M supporting electrolyte [^{n}Bu$_4$N][PF$_6$] referenced to the FeCp$_2^{0/+}$ redox couple at 0.0 V (scan rate = 0.05-0.50 V/s) with full scan window to include small impurity.

8. Single Crystal X-ray Diffraction

Table S8.1: Crystallographic parameters for selected compounds

Compound Name CCDC Entry	[(Tp^{tBu,Me})Ti{≡NSi(CH$_3$)$_3$}(THF)] **2** 2249025	[(Tp^{tBu,Me})TiCl(OEt$_2$)][BC$_6$F$_5$)$_4$] **3^{Et2O}** 2249020	[(Tp^{tBu,Me})TiCl(THF)][BC$_6$F$_5$)$_4$] **3^{THF}** 2249021	[(Tp^{tBu,Me})Ti{≡NSi(CH$_3$)$_3$}(F)] **4** 2249024
Empirical formula	$C_{33.5}H_{63}BN_7OSiTi$	$C_{116}H_{130}B_4Cl_2F_{40}N_{12}O_5Ti_2$	$C_{56}H_{56}B_2ClF_{20}N_6O_2Ti$	$C_{27}H_{49}BFN_7SiTi$
Formula Weight (g/mol)	666.71	2742.25	1330.03	577.53
Temperature (K)	100	100	100	100
Crystal system	monoclinic	triclinic	triclinic	orthorhombic
Spacegroup	$P2_1$	$P\bar{1}$	$P\bar{1}$	Fdd2
a (Å)	11.9991(2)	9.6619(8)	9.6595(6)	60.7204(15)
b (Å)	26.3427(3)	17.3266(14)	16.8693(10)	21.7118(6)
c (Å)	12.1440(2)	18.7101(16)	19.7287(12)	10.0607(2)
α (°)	90	89.065(3)	104.961(2)	90
β (°)	95.9280(10)	85.916(3)	92.699(2)	90
γ (°)	90	83.456(3)	96.031(2)	90
Volume (Å^3)	3818.05(10)	3103.8(4)	3079.4(3)	13263.5(6)
Z	4	1	2	16
ρ_{calc} (g/cm^3)	1.160	1.467	1.434	1.157
μ (mm^{-1})	0.290	0.289	0.289	0.326
F(000)	1448.0	1408.0	1358.0	4960.0
Crystal size (mm^3)	0.28 × 0.22 × 0.2	0.41 × 0.29 × 0.1	0.63 × 0.13 × 0.06	0.5 × 0.4 × 0.02
Radiation wavelength (Å)	0.71073	0.71073	0.71073	0.71073
2θ range (°)	3.71 - 56.306	2.182 - 55.028	2.518 - 54.98°	3.984 - 56.56
Index ranges	$-15 \le h \le 15$, $-34 \le k \le 33$, $-16 \le l \le 16$	$-12 \le h \le 12$, $-22 \le k \le 22$, $-24 \le l \le 22$	$-12 \le h \le 12$, $-21 \le k \le 21$, $-25 \le l \le 25$	$-79 \le h \le 76$, $-26 \le k \le 28$, $-13 \le l \le 12$
Reflections collected	123109	61988	70106	31428
Independent reflections	17709 [R(int) = 0.0577]	14267[R(int) = 0.0560]	70106[R(int) = 0.0514]	7966[R(int) = 0.0306]
Data/restraints/parameters	17709/31/826	14267/28/852	70106/0/806	7966/1/358
Goodness-of-fit on F^2	1.015	1.012	1.033	1.022
Final R indexes [$I \ge 2\sigma$ (I)]	R_1 = 0.0701, wR_2 = 0.1799	R_1 = 0.0521, wR_2 = 0.1057	R_1 = 0.0534, wR_2 = 0.1187	R_1 = 0.0264, wR_2 = 0.0658
Final R indexes [all data]	R_1 = 0.0856, wR_2 = 0.1901	R_1 = 0.0951, wR_2 = 0.1214	R_1 = 0.0689, wR_2 = 0.1249	R_1 = 0.0285, wR_2 = 0.0666
Largest diff. peak/hole (e·Å^3)	1.66/-0.65	0.52/-0.52	0.75/-0.60	0.28/-0.15

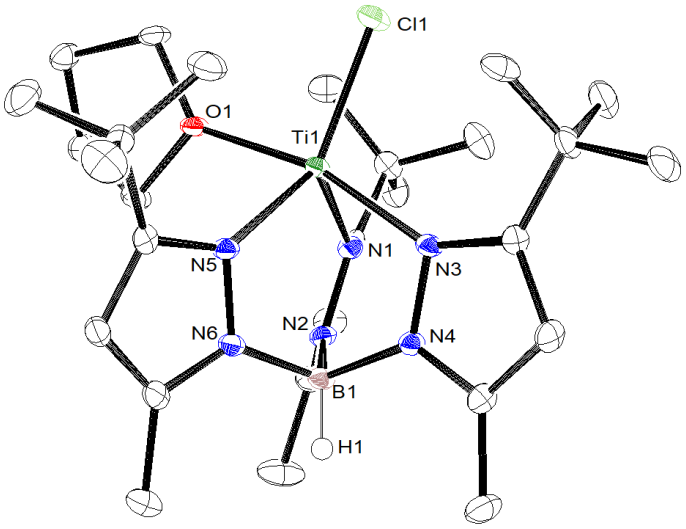

Figure S8.2: Thermal ellipsoid plot (ORTEP-III) of $\mathbf{3}^{\mathbf{THF}}$ (50% probability level). All hydrogen except for apical hydrogen (H1) on boron (B1) have been omitted for clarity. Co-crystallized tetrakis(pentafluorophenyl)borate anion has been removed for clarity. Co-crystallized THF has been omitted for clarity.

9. References

1. S. Trofimenko, *Chem. Rev.*, **1993**, 93, 943-980.
2. N. A. Jones, S. T. Liddle, C. Wilson and P. L. Arnold, *Organometallics*, **2007**, 26, 755-757.
3. A. Reinholdt, D. Pividori, A. L. Laughlin, I. M. DiMucci, S. N. MacMillan, M. G. Jafari, M. R. Gau, P. J. Carroll, J. Krzystek, A. Ozarowski, J. Telser, K. M. Lancaster, K. Meyer and D. J. Mindiola, *Inorg. Chem.,* **2020**, 59, 17834-17850.
4. M. E. Woodhouse, F. D. Lewis, and T. J. Marks, *J. Am. Chem. Soc.,* **1982**, 104, 5586-5594.
5. S. Chakraborty, J. Chattopadhyay, W. Guo and W. E. Billups, *Angew. Chem., Int. Ed.*, **2007**, 46, 4486-4488.
6. D. Alberti and K.-R. Pörschke, *Organometallics*, **2004**, 23, 1459-1460.
7. (a) R. K. Harris, E. D. Becker, S. M. C. d. Menezes, P. Granger, R. E. Hoffman and K. W. Zilm, *Pure Appl. Chem.*, **2008**, 80, 59-84. (b) R. K. Harris, E. D. Becker, S. M. C. d. Menezes, R. Goodfellow and P. Granger, *Pure Appl. Chem.*, **2001**, 73, 1795-1818.
8. (a) D. F. Evans, *J. Chem. Soc.,* **1959**, 2003. (b) S. K. Sur, *J. Mag. Res. (1969)*, **1989**, 82, 169-173.
9. R. Drago, in *Physical Methods for Chemists*, Saunders College Publishing, 2 edn., 1992, ch. 11, pp. 411-434.
10. G. A. Bain and J. F. Berry, *J. Chem. Ed.*, **2008**, 85, 532.
11. N. Elgrishi, K. J. Rountree, B. D. McCarthy, E. S. Rountree, T. T. Eisenhart and J. L. Dempsey, *J. Chem. Ed.,* **2018**, 95, 197-206.
12. Rigaku Oxford Diffraction, *CrysAlisPro*:1.171.42.79a, **2021**, Rigaku Corporation, Oxford, UK
13. Bruker-AXS, *APEX3 2018.1-0*:**2014**, Madison, WI USA
14. *CELL_NOW*:v2008/4,
15. Bruker-AXS, *SAINT*:v8.34A, **2014**, Madison, WI USA
16. Oxford Diffraction Ltd., *SCALE3 ABSPACK*:v1.0.7, **2005**, an Oxford Diffraction program, Abingdon, UK
17. L. Krause, R. Herbst-Irmer, G. M. Sheldrick and D. Stalke, *J. Appl. Cryst.*, **2015**, 48, 3-10.
18. *TWINABS*:v2012/1,
19. G. Sheldrick, *Acta Cryst. A*, SHELXT v2018/2 and SHELXL-2018/3, **2015**, 71, 3-8.
20. A. L. Spek, *Acta. Cryst.*, PLATON (v1100917), **2009**, D65, 148-155.
21. F. P. Gabbaï, P. J. Chirik, D. E. Fogg, K. Meyer, D. J. Mindiola, L. L. Schafer and S.-L. You, *Organometallics*, **2016**, 35, 3255-3256.
22. G. R. Fulmer, A. J. M. Miller, N. H. Sherden, H. E. Gottlieb, A. Nudelman, B. M. Stoltz, J. E. Bercaw and K. I. Goldberg, *Organometallics*, **2010**, 29, 2176-2179.
23. A. J. Rosenthal, M. Devillard, K. Miqueu, G. Bouhadir and D. Bourissou, *Angew. Chem., Int. Ed.*, **2015**, 54, 9198-9202.
24. R. F. C. Calridge, D. G. McGavin and W. C. Tennant, *J. Phys.: Condens. Matter*, **1995**, 7, 9049.